Memo version 1.1

CEPC Analysis Memo

May 5, 2020

Higgs boson decaying to ZZ* channel at the CEPC

Yanxi Gu[a], Min Zhong[a], Lingteng Kong[b], Ryuta Kiuchi[b], Xin Shi[b], Shih-Chieh Hsu[c], and Xinchou Lou[b]

[a]*Department of Modern Physics, University of Science and Technology of China, Hefei, China*
[b]*Institute of High Energy Physics, Beijing 100049, People's Republic of China*
[c]*Department of Physics, University of Washington, Seattle 98195-1560, USA*

Abstract

The precision of the yield measurement of the Higgs boson decaying into two Z bosons process at the Circular Electrion-Positron Collider (CEPC) is evaluated. Including the recoil Z boson associated with the Higgs production (Higgsstrahlung) total three Z bosons involves for this channel, from which final states characterized by the presence of a pair of leptons, quarks, and neutrinos are chosen for the signal. After the event selection, the precision of $\sigma_{ZH}\cdot$Br(H→ZZ) is estimated to be 9.71%.

Contents

ChangeLog

Version 1.2

- 5/05/2020: Add BDT sections (six parallel channels), including event selections and fitting results, as well as some descriptions in Chapter 'AnalysisProcedure'.
- 4/28/2020: Use the unified set of selections.

Version 1.1

- 4/22/2020: 1.Unifying some of the selections and put them in comparison. 2.Modify event-selection table slightly

Version 1.0

- Six parallel channel cut-based event selection
- HZZ branch ratio and its precision

version 0.6

- Change some plot size etc. to make the pdf file after compiling in good order
- Update fitting results (both cut-based and BDT) for 5 channels
- Fill the structure with plots/tables for each channel ("$\mu\mu$", "$\nu\nu$", "qq" channels)

version 0.5

- Update(add) author information
- Change the section numbering so as to start it from the introduction.
- Update the references which was not working, in the introduction section
- Add "Analysis Procedure" section. Add general desription about our analysis framework.
- Make a structure for each channel ("$\mu\mu$", "$\nu\nu$", "qq" channels)

Version 0.4

- Display the result of hvvjj channel

Version 0.4.1

- Add pictures of signal's cut conditions

Version 0.4.2

- Add background distribution

Version 0.4.2

- change samples and update pictures and cut flow table

Version 0.4.3

- 3/19/2019: 1.Update sample table, cut flow table and histograms, now the background in histograms are 2f, 4f and ZH. 2.Add present state of hjjvv channel.

Version 0.4.4

- 4/25/2019: 1.Update results. 2. add equations for calculation

Version 0.4.5

- 5/10/2019: 1.Add introduction. 2. Add more for calculation part

1 Introduction

The historic discovery of a Higgs boson in 2012 by the ATLAS and CMS collaborations [1, 2] at the Large Hadron Collider (LHC) has opened a new era in particle physics. Subsequent measurements of the properties of the new particle have indicated compatibility with the Standard Model (SM) Higgs boson [3, 4, 5, 6, 7, 8, 9]. While the SM has been remarkably successful in describing experimental phenomena, it is important to recognize that it is not a complete theory. In particular, it does not *predict* the parameters in the Higgs potential, such as the Higgs boson mass. The vast difference between the Planck scale and the weak scale remains a major mystery. There is not a complete understanding of the nature of electroweak phase transition. The discovery of a spin zero Higgs boson, the first elementary particle of its kind, only sharpens these questions. It is clear that any attempt of addressing these questions will involve new physics beyond the SM (BSM). Therefore, the Higgs boson discovery marks the beginning of a new era of theoretical and experimental explorations.

A physics program of the precision measurements of the Higgs boson properties will be a critical component of any road map for high energy physics in the coming decades. Potential new physics beyond the SM could lead to observable deviations in the Higgs boson couplings from the SM expectations. Typically, such deviations can be parametrized as

$$\delta = c\frac{v^2}{M_{\mathrm{NP}}^2}, \tag{1}$$

where v and M_{NP} are the vacuum expectation value of the Higgs field and the typical mass scale of new physics, respectively. The size of the proportionality constant c depends on the model, but it should not be much larger than $O(1)$. The high-luminosity LHC (HL-LHC) will measure the Higgs boson couplings to about 5% [10, 11]. At the same time, the LHC will directly search for new physics from a few hundreds of GeV to at least one TeV. Eq. 1 implies that probing new physics significantly beyond the LHC reach would require the measurements of the Higgs boson couplings at least at percent level accuracy. To achieve such precision will need new facilities, a lepton collider operating as a Higgs factory is a natural next step.

The Circular Electron-Positron Collider CEPC, proposed by the Chinese particle physics community, is one of such possible facilities. The CEPC will be placed in a tunnel with a circumference of approximately 100 km and will operate at a center-of-mass energy of $\sqrt{s} \sim 240$ GeV, near the maximum of the Higgs boson production cross section through the $e^+e^- \to ZH$ process. At the CEPC, in contrast to the LHC, Higgs boson candidates can be identified through a technique known as the recoil mass method without tagging its decays. Therefore, the Higgs boson production can be disentangled from its decay in a model independent way. Moreover, the cleaner environment at a lepton collider allows much better exclusive measurements of Higgs boson decay channels. All of these give the CEPC an impressive reach in probing Higgs boson properties. With the expected integrated luminosity of $5.6 fb^{-1}$, over one million Higgs bosons will be produced. With this sample, the CEPC will be able to measure the Higgs boson coupling to the Z boson with an accuracy of 0.25%, more than a factor of 10 better than the LHC. Such a precise measurement gives the CEPC unprecedented reach into interesting new physics scenarios which are difficult to probe at the LHC. The CEPC also has strong capability in detecting Higgs boson invisible decay. It is sensitive to the invisible decay branching ratio down to 0.3%. In addition, it is expected to have good sensitivities to exotic decay channels which are swamped by backgrounds at the LHC. It is also important to stress that an e^+e^- Higgs factory can perform model independent measurement of the Higgs boson width. This unique feature in turn allows for the model independent determination of the Higgs boson couplings.

P.S. Above description given by Lineteng is almost the same as the first section of the CEPC white paper.(2019-12-08)

2 Samples

The analysis is performed on MC samples simulated on the CEPC conceptual detector. Sample path: $/cefs/data/DstData/CEPC240/CEPC\_v4/$, the details of samples is listed below, and the events expected is $5600 fb^{-1}$

Table 1: The alias for particles

$uq : u, \bar{u}$	$up : u, \bar{u}, c, \bar{c}$	$nu_e : \nu_e, \overline{\nu}_e$
$dq : d, \bar{d}$	$down : d, \bar{d}, s, \bar{s}, b, \bar{b}$	$nu_\mu : \nu_\mu, \overline{\nu}_\mu$
$cq : c, \bar{c}$	$e : e^-, e^+$	$nu_\tau : \nu_\tau, \overline{\nu}_\tau$
$sq : s, \bar{s}$	$mu : \mu^-, \mu^+$	$nu_{\mu,\tau} : \nu_{\mu,\tau}, \overline{\nu}_{\mu,\tau}$
$bq : b, \bar{b}$	$tau : \tau^-, \tau^+$	$nu : \nu_{e,\mu,\tau}, \overline{\nu}_{e,\mu,\tau}$
$f : e^-, \mu, \tau, \nu_e, \nu_\mu, \nu_\tau, u, d, c, s, b$		q:u,d,c,s,b

2.1 ZH Samples

Table 2: ZH sample list

Process	Cross section	Events expected
e1e1h_aa	0.0161	90.24855
e1e1h_az	0.0108	60.5394
e1e1h_bb	4.06	22758.33
e1e1h_cc	0.205	1149.1275
e1e1h_e2e2	0.00154	8.63247
e1e1h_e3e3	0.445	2494.4475
e1e1h_gg	0.603	3380.1165
e1e1h_ss	0.0	0.0
e1e1h_ww	1.51	8464.305
e1e1h_zz	0.186	1042.623
e2e2h_aa	0.0154	86.3247
e2e2h_az	0.0104	58.2972
e2e2h_bb	3.91	21917.505
e2e2h_cc	0.197	1104.2835
e2e2h_e2e2	0.00148	8.29614
e2e2h_e3e3	0.428	2399.154
e2e2h_gg	0.58	3251.19
e2e2h_ss	0.0	0.0
e2e2h_ww	1.46	8184.03
e2e2h_zz	0.179	1003.3845
e3e3h_aa	0.0154	86.3247
e3e3h_az	0.0103	57.73665
e3e3h_bb	3.89	21805.395
e3e3h_cc	0.196	1098.678
e3e3h_e2e2	0.00148	8.29614
e3e3h_e3e3	0.427	2393.5485
e3e3h_gg	0.578	3239.979
e3e3h_ss	0.0	0.0
e3e3h_ww	1.45	8127.975
e3e3h_zz	0.178	997.779
nnh_aa	0.106	594.183
nnh_az	0.0708	396.8694
nnh_bb	26.7	149666.85
nnh_cc	1.35	7567.425
nnh_e2e2	0.0101	56.61555
nnh_e3e3	2.93	16424.115
nnh_gg	3.97	22253.835
nnh_ss	0.0	0.0
nnh_ww	9.95	55774.725
nnh_zz	1.22	6838.71
qqh_aa	0.312	1748.916
qqh_az	0.209	1171.5495
qqh_bb	78.9	442273.95
qqh_cc	3.98	22309.89
qqh_e2e2	0.03	168.165
qqh_e3e3	8.65	48487.575
qqh_gg	11.7	65584.35
qqh_ss	0.0	0.0
qqh_ww	29.4	164801.7
qqh_zz	3.61	20235.855

2.2 Two fermions background Samples

Table 3: General information about two fermions background samples

Process	Cross section	Events expected
qq	54106.86	303296003.73
e2e2	5332.71	29892506.46
e3e3	4752.89	26642325.45
e1e1	24770.9	138853279.95
n1n1	45390.79	254438073.9
n2n2	4416.3	24755569.65
n3n3	4410.26	24721712.43

2.3 Four fermions background Samples

Table 4: General information about four fermions background samples

Process	Cross section	Events expected
zz_h0utut	85.68	480279.24
zz_h0dtdt	233.46	1308660.03
zz_h0uu_notd	98.56	552478.08
zz_h0cc_nots	98.97	554776.89
zz_sl0nu_up	84.38	472992.09
zz_sl0nu_down	139.71	783144.96
zz_sl0mu_up	87.39	489865.2
zz_sl0mu_down	136.14	763132.77
zz_sl0tau_up	41.56	232964.58
zz_sl0tau_down	67.31	377306.76
zz_l04tau	4.61	25841.91
zz_l04mu	15.56	87221.58
zz_l0taumu	18.56	104038.08
zz_l0mumu	19.38	108634.59
zz_l0tautau	9.61	53869.41
ww_h0cuxx	3478.89	19500918.45
ww_h0uubd	0.05	280.83
ww_h0uusd	170.45	955458.03
ww_h0ccbs	5.89	33016.95
ww_h0ccds	170.18	953943.99
ww_sl0muq	2423.43	13584537.42
ww_sl0tauq	2423.56	13585265.58
ww_l0ll	403.66	2262716.13
zzorww_h0udud	1610.32	9026648.76
zzorww_h0cscs	1607.55	9011122.08
zzorww_l0mumu	221.1	1239376.05
zzorww_l0tautau	211.18	1183769.49
sze_l0tau	147.28	825578.04
sze_l0mu	845.81	4741188.51
sze_l0nunu	28.94	162223.17
sze_sl0uu	190.21	1066222.71
sze_sl0dd	125.83	705340.62
sznu_l0mumu	43.42	243390.81
sznu_l0tautau	14.57	81672.69
sznu_sl0nu_up	55.59	311610.3
sznu_sl0nu_down	90.03	504663.72
sw_l0mu	436.7	2447921.85
sw_l0tau	435.93	2443606.17
sw_sl0qq	2612.62	14645041.41
szeorsw_l0l	249.48	1398460.14

3 Analysis Procedure

We give here a brief explanation about the analysis framework which is common to all of indivisual channels. The Marlin framework is used for this flow.

The analysis starts from the reconstructed objects as inputs. The lepton isolation processor, the jet clustering processor are applied on the Arbor PFO to separate leptons from the rest. The remain objects are going to be clustered into number of jets by the the jet clustering processor, where we can designate the jet algorithm to be used, the number of (exclusive) jets and so on. Classified objects are feed into a processor which we call it internally as “Higgs2zz” processor and pre selection on events are performed. Fig. 1 is the skematic of the analysis flow chart, and further details are given in the following items.

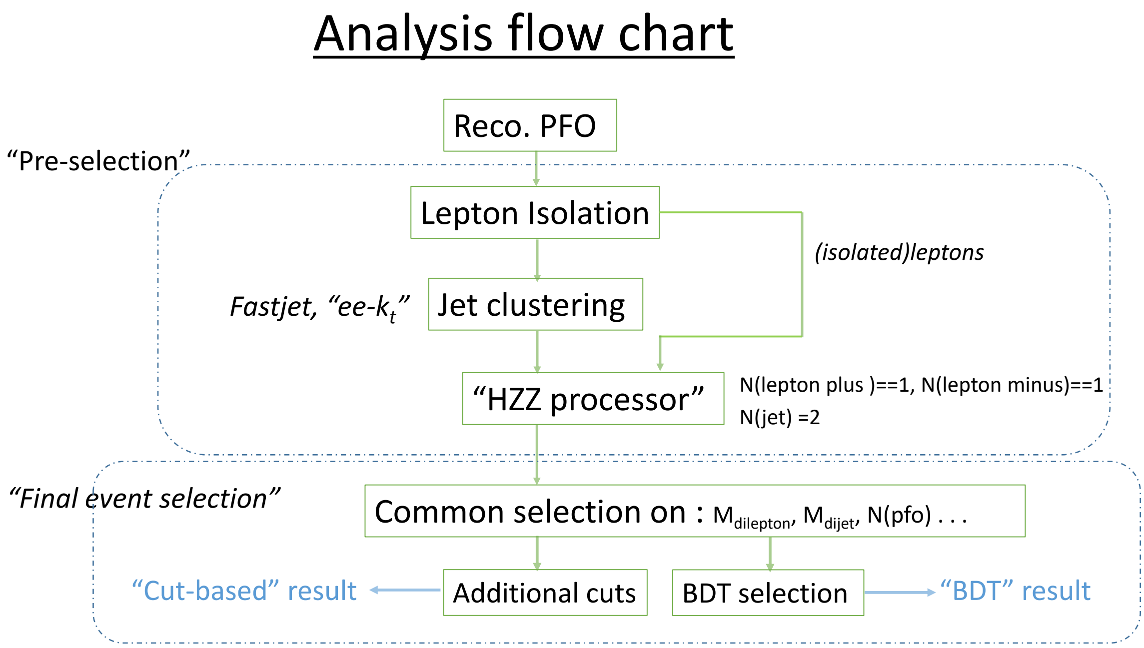

Figure 1: Analysis Flow Chart

Lepton Isolation

The leptons, here they are electrons and muons, like the decay particles of the initial Z boson, should not be merged into jets, and the task is done by this lepton isoloation processor. The isolated status is judged from several condistions, such as particles having “cone energy” which is lower than certain thredhold, as well as requiring its PID as that of electrons or muons. The input collection to the processor is the Arbor PFO, and it has two output collections, one includes only isolated leptons, the other includes the rest.

Jet Clustering

FastJet processor has been chosen for the jet clustering process. We have used so-called "ee-kt" algorithm. The input collection is the one which does not include isolated leptons, and that is clustered into two jets exclusively, by setting the number of jets option as two. The output collection of this processor has information of these two jets.

Event Preselection

The "Higgs2zz" processor has role of the event preselection. The input collections consists of output of the lepton isolation processor for the isolated leptons, output of the fastjet processor for the jets, the Arbor PFO collection and the MCParticle collection for MC truth information. If event contains one positive charged lepton and one minus charged lepton in the isolated lepton collection, and the two jets from the fastjet processor, this event is saved. Several meaningful information, such as di lepton mass and momentum, are obtained at this stage and as well.

BDT Selection

After several common selections ($M_{Higgscandidate}$, $M^{recoil}_{Higgscandidate}$, $N(pfo)$ and $cos\ \theta_{visible}$), the size of signal and background samples is suppressed to appropriate size to be the input files of BDT study. The cut values are mainly determined by the cut-based study.

The python method scikit-learn is used here instead of TMVA for BDT study. Some details about the BDT could be found in Table 5. In the case of number of signal events much less than the background events, to get better BDT performance, imbalanced learn method is applied.

When the BDT training is finished, the output BDT model could be used to calculate a BDT score for each event with the input variable list. Once the distribution of this BDT score is available, we could apply a cut on the BDT score (default value is 0.00). To determine which value is the best, the $\frac{S}{\sqrt{S+B}}$ versus cut value curve will be shown for each channel.

Typical distribusions after this pre selection process on $\mu\mu$HZZ signal sample are shown in Fig. 2-3. Corresponding description about the histograms should be given briefly here.

Table 5: Some settings and parameters of Boosted Decision Tree (BDT).

Setting	Value
Type of classifier	AdaBoost
Algorithm	SAMME
Number of estimators	800
Learning rate	0.5
Test/Train sample size ratio	1
Max depth	1
Min samples leaf	10
Min samples split	20

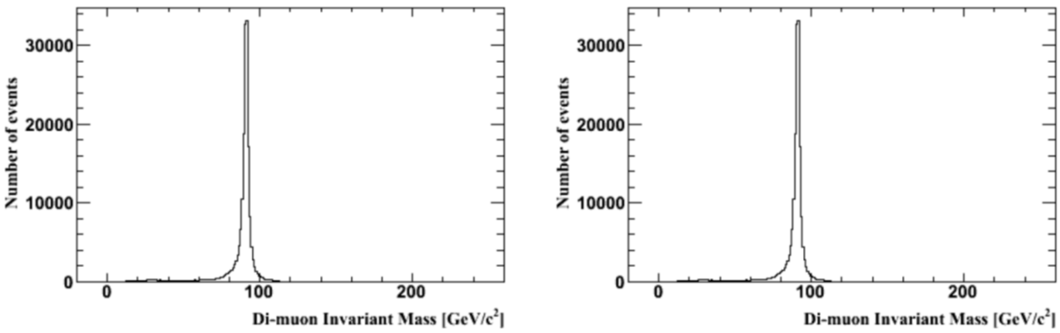

Figure 2: Distributions of the invariant mass and the recoil mass of di-muons. The figures shall be updated. .

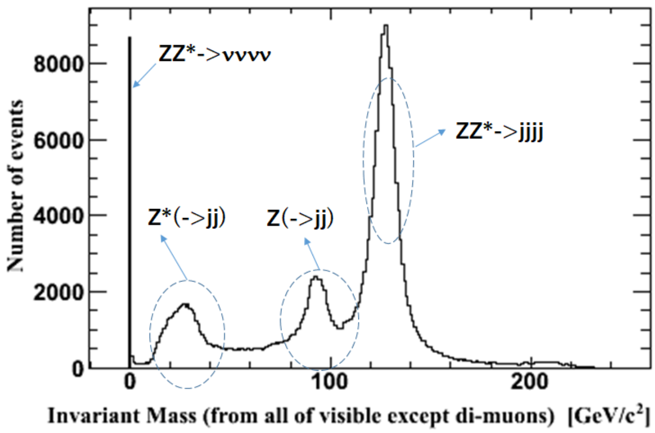

Figure 3: Visible (but except the di-muons) mass distribution. Or, di-jet invariant mass distribution.. The figures shall be updated. .

4 Event Selection of Z(→$\mu\mu$)H(ZZ*→$\nu\nu qq$)

4.1 Z(→ $\mu^+\mu^-$), H(Z→$\nu\bar{\nu}$, Z*→$q\bar{q}$)

4.1.1 Event selection (Cut-based only)

Table 6: Cut flow table for $\mu\mu\nu\nu qq$ channel

Cut	Signal	ZH Background	2f Background	4f Background	$\frac{S}{\sqrt{S+B}}$
$Expected$	1000.88±31.64	1140511±1067	801811977±28316	107203890±10353	
$Pre-selection$	616.68±24.83	30494 ±174	480828±693	515448±717	
$Signal\ or\ not$	211.44±14.54	30282 ±174	480828±693	515448±717	
$M_{missing} > M_{dijet}$	107.97±10.39	1608 ±40	115062±339	28809 ±169	0.283
$N(pfo)$	104.16±10.21	908 ±30	33480 ±182	14159 ±118	0.4722
M_{dimuon}	92.43 ±9.61	296 ±17	24151 ±155	1625 ±40	0.5714
M_{dijet}	87.58 ±9.36	280 ±16	851 ±29	819 ±28	1.9395
$M_{missing}$	71.98 ±8.48	124 ±11	97 ±9	101 ±10	3.6196
$*cos\ \theta$	71.98 ±8.48	124 ±11	97 ±9	101 ±10	3.6196
$cos\theta_{visible}$	68.7 ±8.29	118 ±10	22 ±4	39 ±6	4.349
$Angle_{\mu j}$	62.43 ±7.9	95 ±9	14 ±3	20 ±4	4.4919
M^{rec}_{dimuon}	61.2 ±7.82	79 ±8	14 ±3	8 ±2	4.7795
M^{rec}_{dijet}	59.24 ±7.7	69 ±8	0 ±0	4 ±2	5.1374
$*M_{visible}$	59.24 ±7.7	69 ±8	0 ±0	4 ±2	5.1374
$*P_{visible}$	59.24 ±7.7	69 ±8	0 ±0	4 ±2	5.1374
$*P_{T_{visible}}$	59.24 ±7.7	69 ±8	0 ±0	4 ±2	5.1374
$*E_{leading\ jet}$	59.24 ±7.7	69 ±8	0 ±0	4 ±2	5.1374
$*P_{T_{leading\ jet}}$	59.24 ±7.7	69 ±8	0 ±0	4 ±2	5.1374
$*E_{sub-leading\ jet}$	59.24 ±7.7	69 ±8	0 ±0	4 ±2	5.1374
$*P_{T_{sub-leading\ jet}}$	59.24 ±7.7	69 ±8	0 ±0	4 ±2	5.1374
$not\ qqHZZ$	59.24 ±7.7	69 ±8	0 ±0	4 ±2	5.1374
$not\ \nu\nu HZZ$	50.14 ±7.08	36 ±6	0 ±0	4 ±2	5.2503±0.5793

The event selection cuts are listed below in sequence.

- $M_{miss} > M_{dijets}$: the missing mass is greater than the dijet invariant mass.

- $20 < N_{pfo} < 90$: Number of Prticle Flow Objects should be in this range.

- $80GeV < M_{\mu^+\mu^-} < 100GeV$: the invariant mass of the dimuon should be in this range.

- $15GeV < M_{dijet} < 60GeV$: the invariant mass of dijet should be in this range.

Table 7: Remained backgrounds (more than 1 event) after all of cuts applied.

name	scale	final
e2e2h_e3e3	0.023968	2
e2e2h_ww	0.08176	22
nnh_zz	0.06832	10
zz_sl0mu_down	1.08025726079	1
zz_sl0tau_up	1.10880522921	1
zz_l0taumu	1.0404004004	2

Table 8: Remained backgrounds (more than 1 event) before final two cuts applied.

name	scale	final
e2e2h_e3e3	0.023968	2
e2e2h_ww	0.08176	24
nnh_zz	0.06832	41
zz_sl0mu_down	1.08025726079	1
zz_sl0tau_up	1.10880522921	1
zz_l0taumu	1.0404004004	2

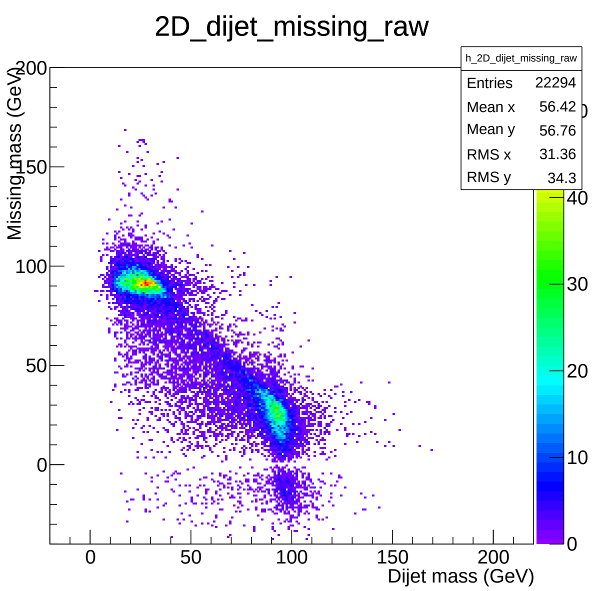

Figure 4: Missing mass vs dijet invariant mass.

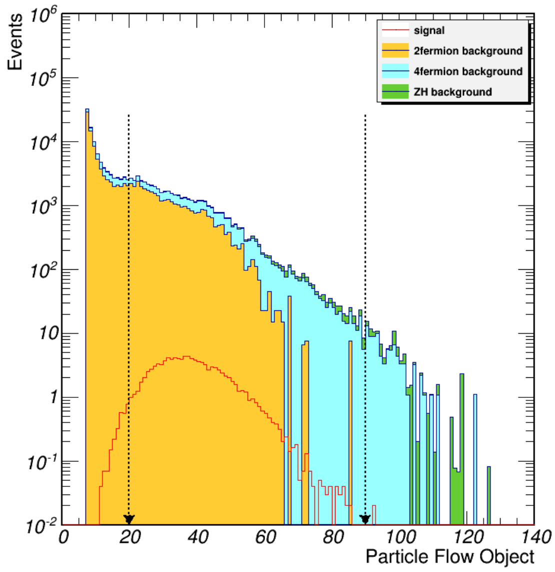

Figure 5: Number of PFOs.

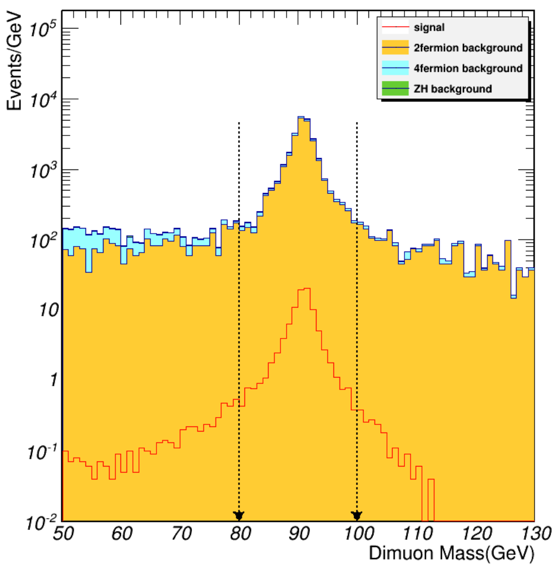

Figure 6: Invariant mass of di-muons.

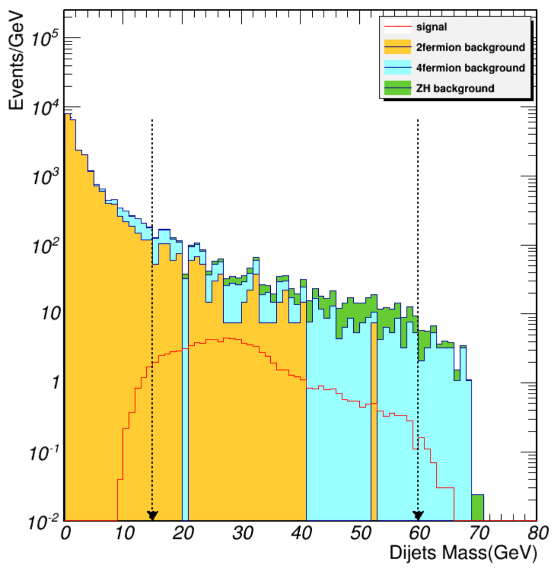

Figure 7: Invariant mass of di-jets.

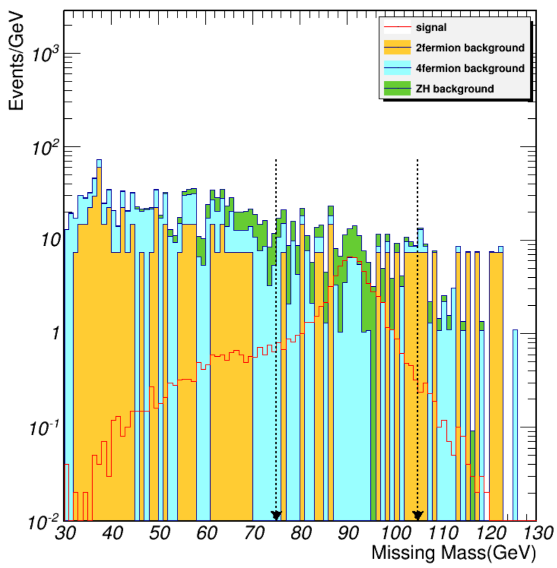

Figure 8: Recoil mass of visible particles.

- $75GeV < M_{visible}^{Recoil} < 105GeV$: the recoil mass of all visible particles should be in this range.

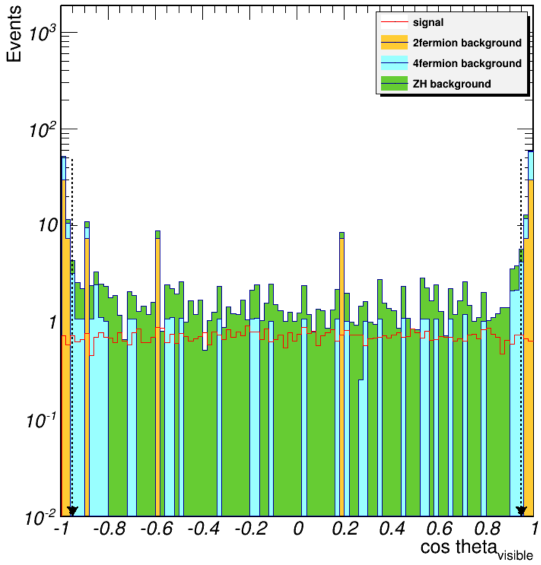

Figure 9: All visible particle $cos\ \theta$

- $-0.95 < cos\ \theta_{visible} < 0.95$: $cos\theta$ of the summation of all visible particles should be in this range.

- $60 < Min\ angle < 170°$: Minimum angle between the two Z(Z*) reconstructed by leptons and jets should be within this range .

- $110GeV < M_{Recoil}^{dimuon} < 140GeV$: the recoil mass of the dimuon should be in this range.

- $185GeV < M_{Recoil}^{dijet} < 220GeV$: the recoil mass of the dijet should be in this range.

Two additional cuts:

- $M_{dijet}^{rec} < 122GeV\ or\ M_{dijet}^{rec} > 128GeV$: To avoid the overlap events with qqHZZ signals.
- $M_{visible} < 122GeV\ or\ M_{visible} > 128GeV$: To remove the overlap events with $\nu\nu$HZZ signals.

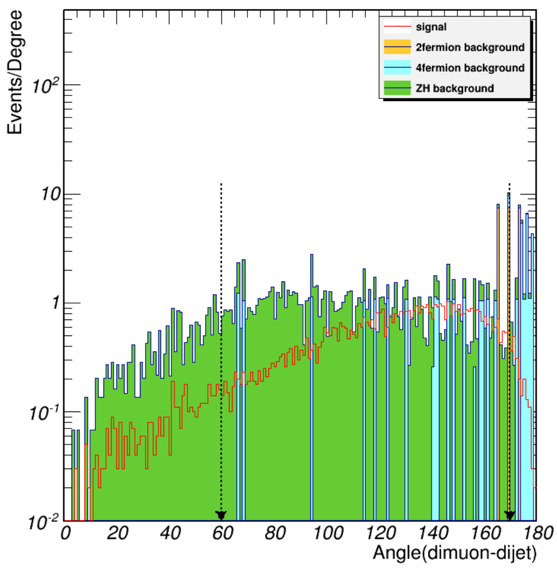

Figure 10: Minimum angle between the two Z(Z*) reconstructed by leptons and jets.

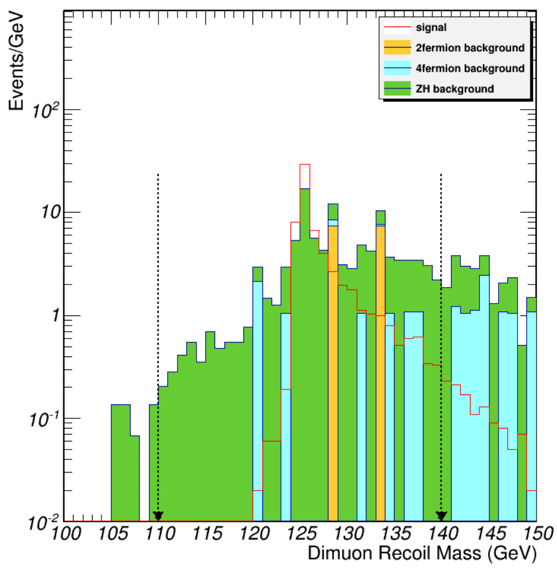

Figure 11: Recoil mass of di-muons.

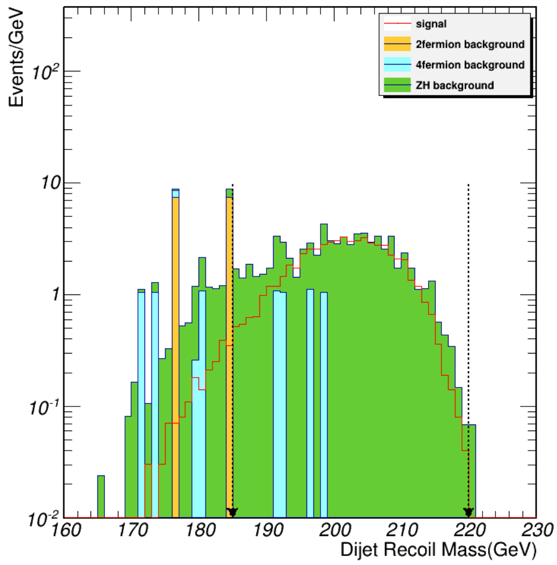

Figure 12: Recoil mass of di-jets.

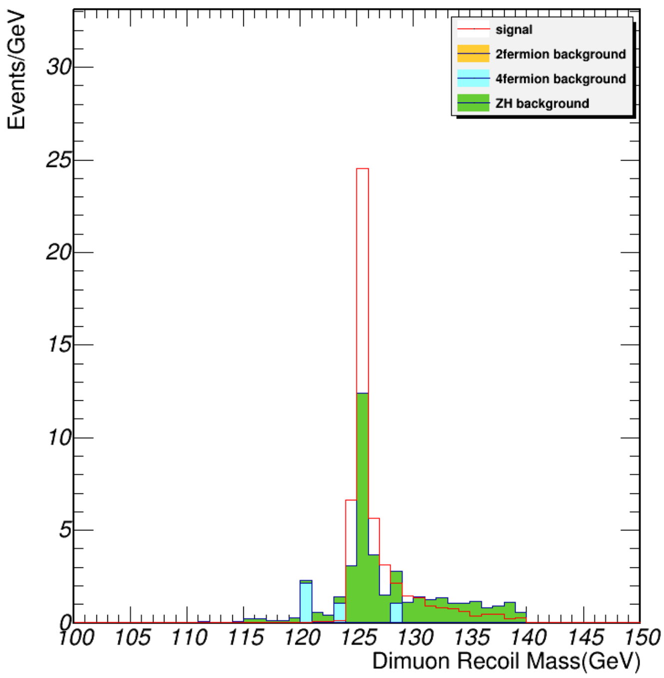

Figure 13: Distribution of the recoil mass of dimuon, after all of cuts applied.

4.1.2 Event selection combined with BDT method

Table 9: Cut flow table for $\mu\mu\nu\nu qq$ channel with BDT

Cut	Signal	ZH Background	2f Background	4f Background	$\frac{S}{\sqrt{S+B}}$
$Expected$	1000	1140511	801811977	107203890	
$Pre-selection$	616	30494	480828	515424	
$Signal\ or\ not$	211	30282	480828	515424	
$M_{missing} > M_{dijet}$	107	1608	115062	28811	0.2830
$N(pfo)$	104	908	33480	14161	0.4722
M_{dimuon}	92	296	24151	1629	0.5714
M^{rec}_{dimuon}	89	256	1642	406	1.8279
$cos\ \theta_{visible}$	85	240	388	127	2.9422
$BDT\ score$	45	6	0	2	6.1727

- $M_{missing} > M_{dijet}$: the missing mass is greater than the dijet invariant mass.
- $20 < N_{pfo} < 90$: Number of PFO is greater than 20 and less than 90.
- $80GeV < M_{\mu^+\mu^-} < 100GeV$: the invariant mass of dimuon should be in this range.
- $110GeV < M^{rec}_{dimuon} < 140GeV$: the recoil mass of the dimuon should be in this range.
- $-0.95 < cos\ \theta_{visible} < 0.95$: $cos\theta$ of the summation of all visible particles should be in this range.
- $BDT\ score > 0.15$: BDT score greater than 0.15.

Table 10: Remained backgrounds (more than 1 event) after all of cuts applied.

name	scale	final
e2e2h_ww	0.08176	3
nnh_zz	0.06832	2
zz_sl0mu_down	1.08025726079	1
zz_sl0tau_up	1.10880522921	1

The input variable list is: M_{dimuon}, M_{dijet}, $M_{missing}$, N_{pfo}, $cos\ \theta$, $cos\ \theta_{visible}$, $Angle_{\mu^+\mu^- - dijet}$, M^{rec}_{dijet}, $M_{visible}$, $P_{visible}$, $P_{T_{visible}}$, $E_{leading\ jet}$, $P_{T_{leading\ jet}}$, $E_{sub-leading\ jet}$, $P_{T_{sub-leading\ jet}}$. All the variables that are used in cut-based study are in the input variable list for BDT, except M^{rec}_{dimuon}, since it is the final observable.

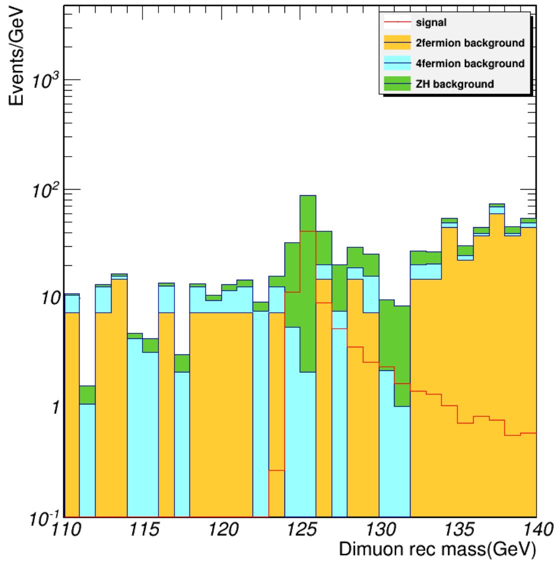

Figure 14: Distribution of the recoil mass of dimuon, after the previous cuts applied, before BDT decision applied.

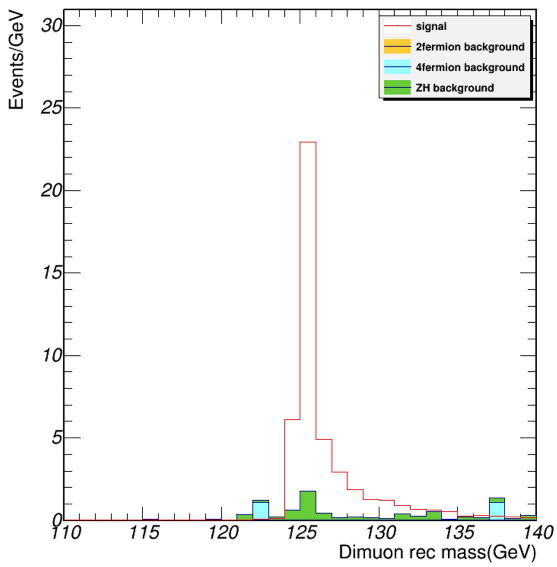

Figure 15: Distribution of the recoil mass of dimuon, after all of cuts & BDT decision applied.

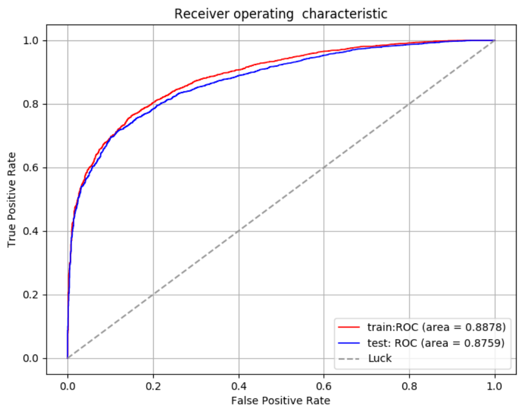

Figure 16: Receiver Operating Characteristic (ROC) curve.

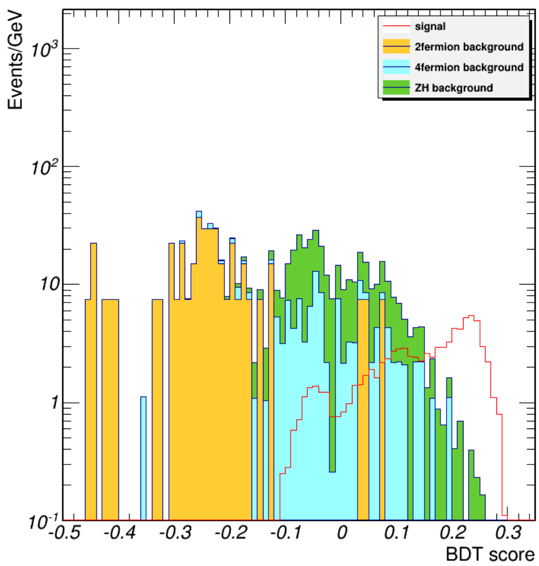

Figure 17: Classifier output distributions of signal and background.

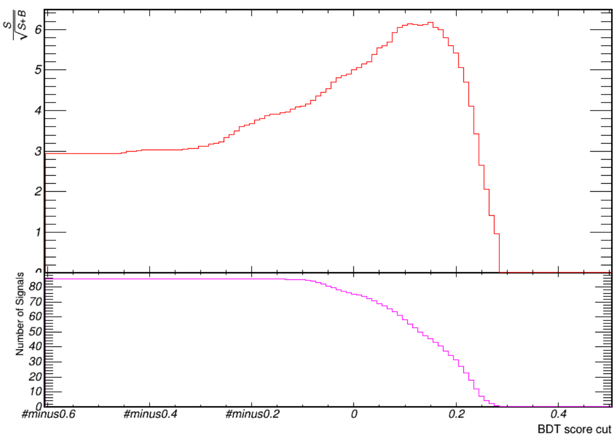

Figure 18: $\frac{S}{\sqrt{S+B}}$ vs BDT score curve.

4.2 Z($\rightarrow \mu^+\mu^-$), H(Z$\rightarrow q\bar{q}$, Z*$\rightarrow \nu\bar{\nu}$)

4.2.1 Event selection (Cut-based only)

Table 11: Cut flow table for $\mu\mu qq\nu\nu$ channel

Cut	Signal	ZH Background	2f Background	4f Background	$\frac{S}{\sqrt{S+B}}$
$Expected$	1000.88±31.64	1140511±1067	801811977±28316	107203890±10353	
$Pre-selection$	616.68±24.83	30494 ±174	480828±693	515448±717	
$Signal\ or\ not$	211.44±14.54	30282 ±174	480828±693	515448±717	
$M_{missing} < M_{dijet}$	103.46±10.17	28674 ±169	365766±604	486638±697	0.1102
$N(pfo)$	100.24±10.01	21686 ±147	12184 ±110	332162±576	0.1657
M_{dimuon}	89.98 ±9.49	16833 ±129	9085 ±95	207927±455	0.186
M_{dijet}	82.95 ±9.11	2768 ±52	52 ±7	173775±416	0.1974
$M_{missing}$	71.56 ±8.46	1679 ±40	14 ±3	13434 ±115	0.5804
$*cos\ \theta$	71.56 ±8.46	1679 ±40	14 ±3	13434 ±115	0.5804
$cos\theta_{visible}$	67.99 ±8.25	1535 ±39	0 ±0	8545 ±92	0.6749
$Angle_{\mu j}$	60.89 ±7.8	1187 ±34	0 ±0	2233 ±47	1.0321
M^{rec}_{dimuon}	59.24 ±7.7	1111 ±33	0 ±0	965 ±31	1.2816
$*M^{rec}_{dijet}$	59.24 ±7.7	1111 ±33	0 ±0	965 ±31	1.2816
$M_{visible}$	55.35 ±7.44	966 ±31	0 ±0	805 ±28	1.295
$*P_{visible}$	55.35 ±7.44	966 ±31	0 ±0	805 ±28	1.295
$*P_{T_{visible}}$	55.35 ±7.44	966 ±31	0 ±0	805 ±28	1.295
$*E_{leading\ jet}$	55.35 ±7.44	966 ±31	0 ±0	805 ±28	1.295
$*P_{T_{leading\ jet}}$	55.35 ±7.44	966 ±31	0 ±0	805 ±28	1.295
$*E_{sub-leading\ jet}$	55.35 ±7.44	966 ±31	0 ±0	805 ±28	1.295
$*P_{T_{sub-leading\ jet}}$	55.35 ±7.44	966 ±31	0 ±0	805 ±28	1.295
$not\ qqHZZ$	48.0 ±6.93	774 ±27	0 ±0	659 ±25	1.247
$not\ \nu\nu HZZ$	48.0 ±6.93	774 ±27	0 ±0	659 ±25	1.247 ±0.3089

The event selection cuts are listed below in sequence.

- $M_{miss} > M_{dijets}$: the missing mass is greater than the dijet invariant mass.

- $30 < N_{pfo} < 100$: Number of Prticle Flow Objects should be in this range.

- $80GeV < M_{\mu^+\mu^-} < 100GeV$: the invariant mass of the dimuon should be in this range.

- $60GeV < M_{dijet} < 105GeV$: the invariant mass of dijet should be in this range.

Table 12: Remained backgrounds (more than 1 event) after all of cuts applied.

name	scale	final
e2e2h_bb	0.21896	419
e2e2h_cc	0.011032	5
e2e2h_e3e3	0.023968	5
e2e2h_gg	0.0326888819557	1
e2e2h_ww	0.08176	303
e2e2h_zz	0.010024	6
e3e3h_zz	0.009968099681	1
qqh_e3e3	0.4844	7
qqh_ww	1.6464	1
qqh_zz	0.20216	21
zz_sl0mu_up	1.09032214858	159
zz_sl0mu_down	1.08025726079	488
zz_sl0tau_down	1.10887174477	5
ww_sl0muq	1.2235862395	6

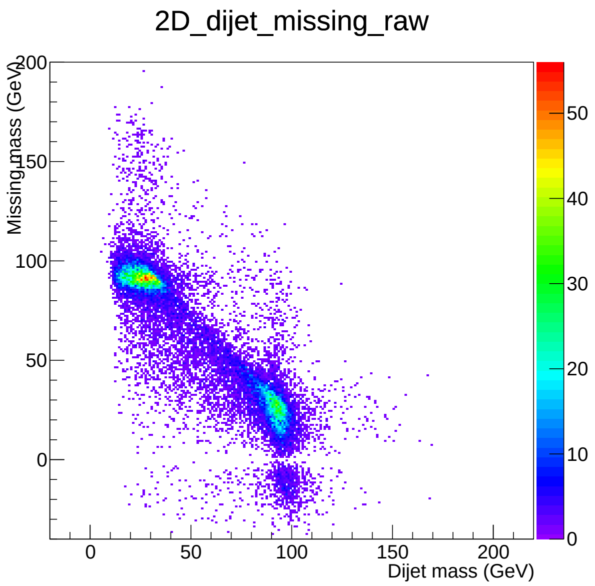

Figure 19: Missing mass vs dijet invariant mass.

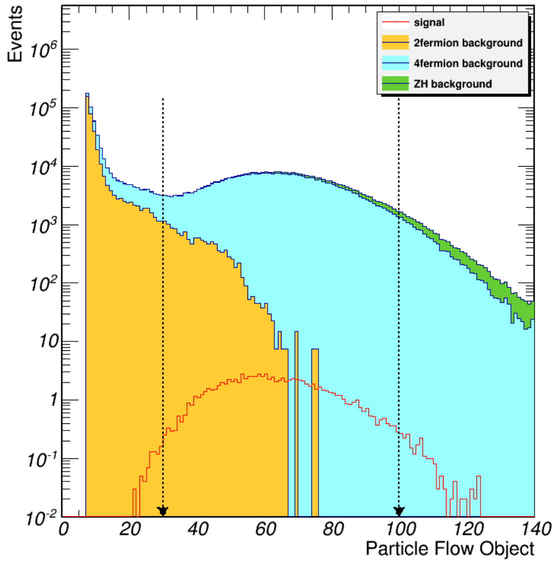

Figure 20: Number of PFOs.

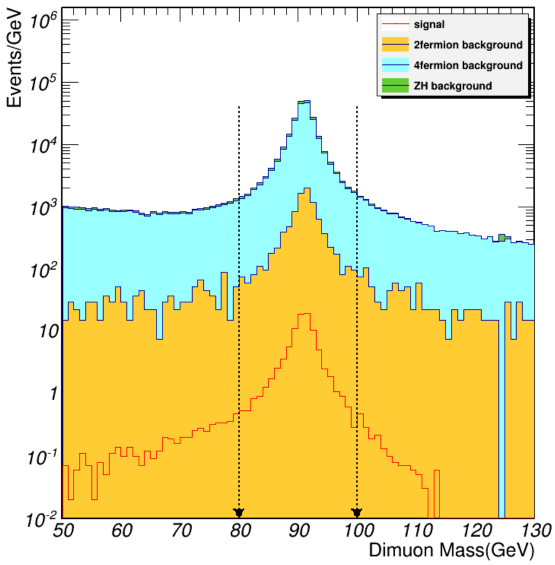

Figure 21: Invariant mass of di-muons.

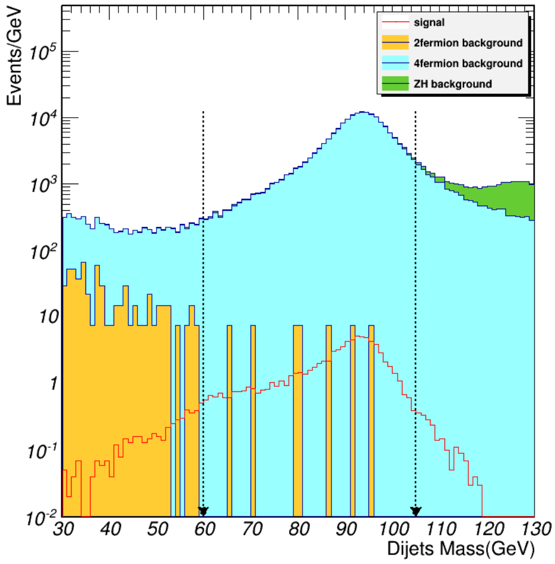

Figure 22: Invariant mass of di-jets.

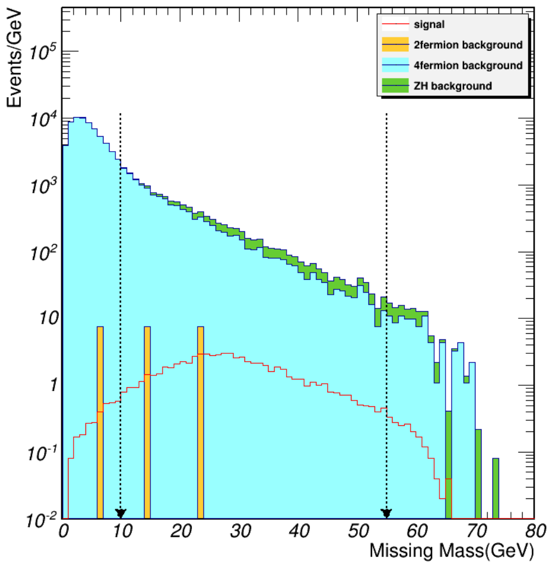

Figure 23: Recoil mass of visible particles.

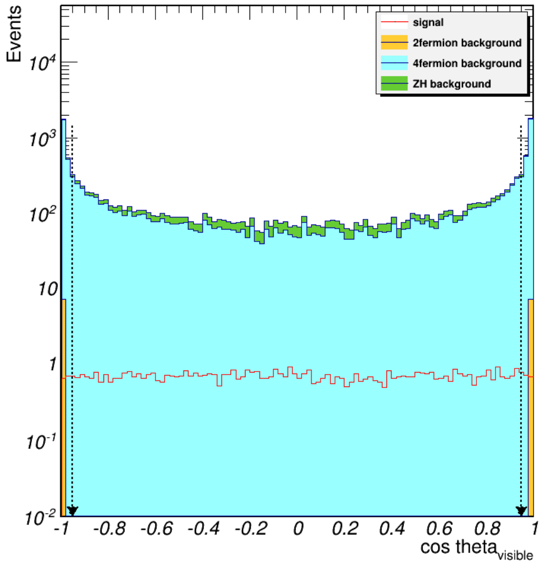

Figure 24: All visible particle $cos\ \theta$

- $10GeV < M_{visible}^{Recoil} < 55GeV$: the recoil mass of all visible particles should be in this range.

- $-0.95 < cos\ \theta_{visible} < 0.95$: $cos\theta$ of the summation of all visible particles should be in this range.

- $60 < Min\ angle < 170°$: Minimum angle between the two Z(Z*) reconstructed by leptons and jets should be within this range .

- $110GeV < M_{Recoil}^{dimuon} < 140GeV$: the recoil mass of the dimuon should be in this range.

- $175GeV < M_{visible} < 215GeV$: the visible mass of all particles should be in this range.

Two additional cuts:

- $M_{dijet}^{rec} < 122GeV\ or\ M_{dijet}^{rec} > 128GeV$: To avoid the overlap events with qqHZZ signals.
- $M_{visible} < 122GeV\ or\ M_{visible} > 128GeV$: To remove the overlap events with $\nu\nu$HZZ signals.

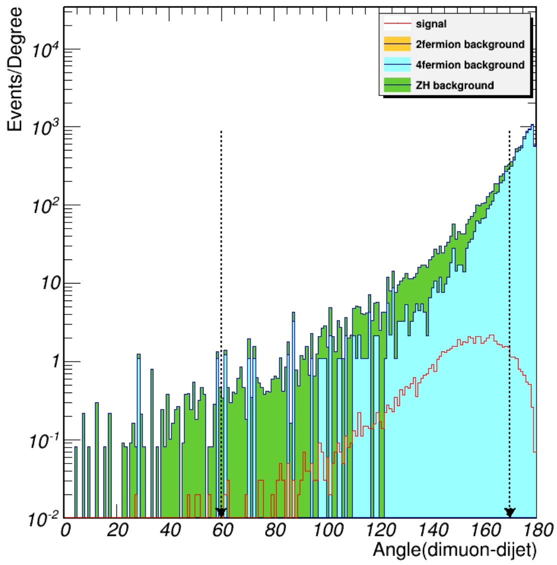

Figure 25: Minimum angle between the two Z(Z*) reconstructed by leptons and jets.

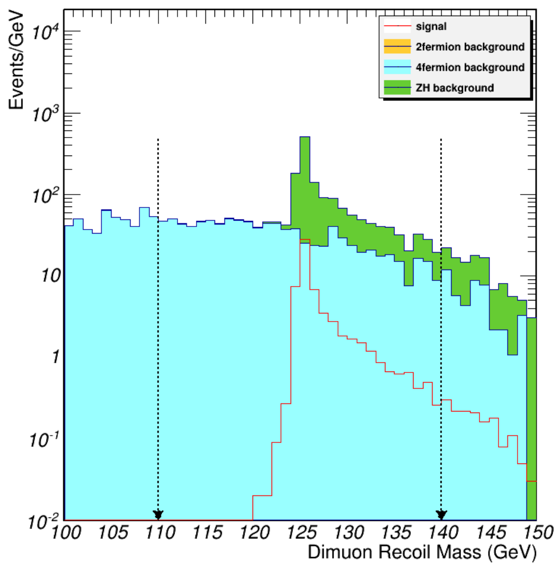

Figure 26: Recoil mass of di-muons.

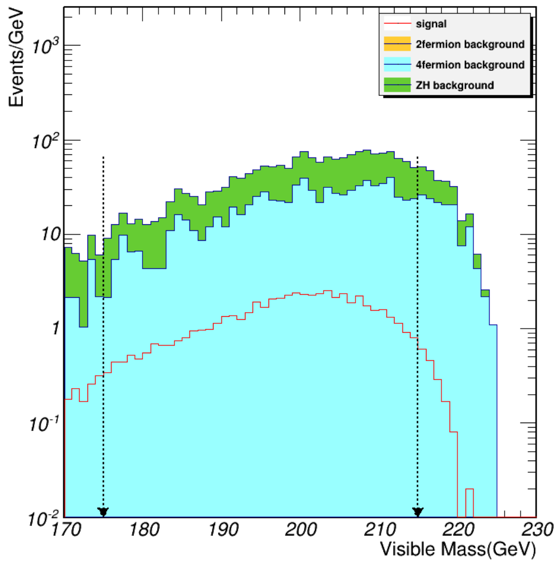

Figure 27: Visible mass of all particles.

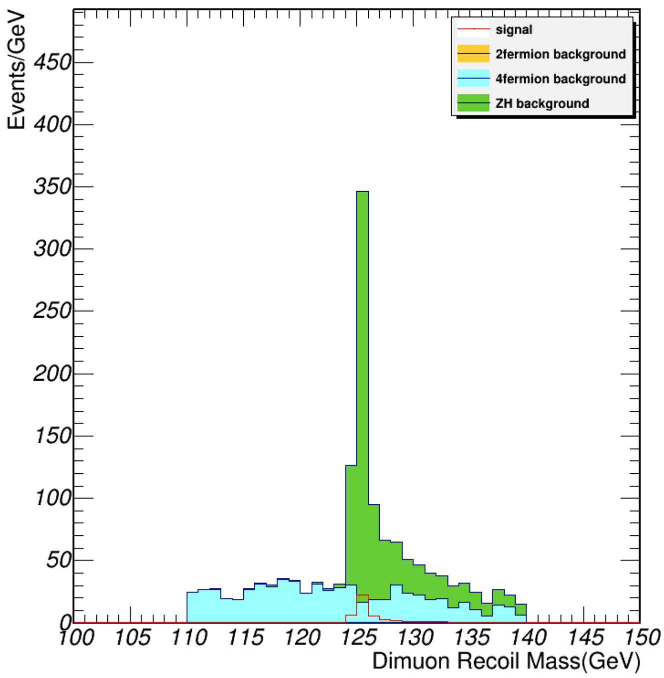

Figure 28: Distribution of the recoil mass of dimuon, after all of cuts applied.

4.2.2 Event selection combined with BDT method

Table 13: Cut flow table for $\mu\mu qq\nu\nu$ channel with BDT

Cut	Signal	ZH Background	2f Background	4f Background	$\frac{S}{\sqrt{S+B}}$
$Expected$	1000	1140511	801811977	107203890	
$Pre-selection$	616	30494	480828	515424	
$Signal\ or\ not$	211	30282	480828	515424	
$M_{missing} < M_{dijet}$	103	28674	365766	486613	0.1102
$N(pfo)$	100	21686	12184	332136	0.1657
M_{dimuon}	89	16833	9085	207927	0.186
M^{rec}_{dimuon}	87	16144	321	25675	0.4236
$cos\ \theta_{visible}$	82	14667	0	12539	0.4992
$BDT\ score$	54	806	0	605	1.4262

- $M_{missssing} < M_{dijet}$: the missing mass is smaller than the dijet invariant mass.
- $30 < N_{pfo} < 100$: Number of PFO is greater than 30 and less than 100.
- $80GeV < M_{\mu^+\mu^-} < 100GeV$: the invariant mass of dimuon should be in this range.
- $110GeV < M^{rec}_{dimuon} < 140GeV$: the recoil mass of the dimuon should be in this range.
- $-0.95 < cos\ \theta_{visible} < 0.95$: $cos\theta$ of the summation of all visible particles should be in this range.
- $BDT\ score > 0.03$: BDT score greater than 0.03.

Table 14: Remained backgrounds (more than 5 event) after all of cuts applied.

name	scale	final
e2e2h_bb	0.21896	448
e2e2h_cc	0.011032	5
e2e2h_ww	0.08176	298
e2e2h_zz	0.010024	5
qqh_e3e3	0.4844	11
qqh_zz	0.20216	30
zz_sl0mu_up	1.09032214858	127
zz_sl0mu_down	1.08025726079	455
zz_sl0tau_down	1.10887174477	5
ww_sl0muq	1.10890944134	13

The input variable list is: M_{dimuon}, M_{dijet}, $M_{missing}$, N_{pfo}, $cos\ \theta$, $cos\ \theta_{visible}$, $Angle_{\mu^+\mu^- - dijet}$, M^{rec}_{dijet}, $M_{visible}$, $P_{visible}$, $P_{T_{visible}}$, $E_{leading\ \ jet}$, $P_{T_{leading\ \ jet}}$, $E_{sub-leading\ \ jet}$, $P_{T_{sub-leading\ \ jet}}$. All the variables that are used in cut-based study are in the input variable list for BDT, except M^{rec}_{dimuon}, since it is the final observable.

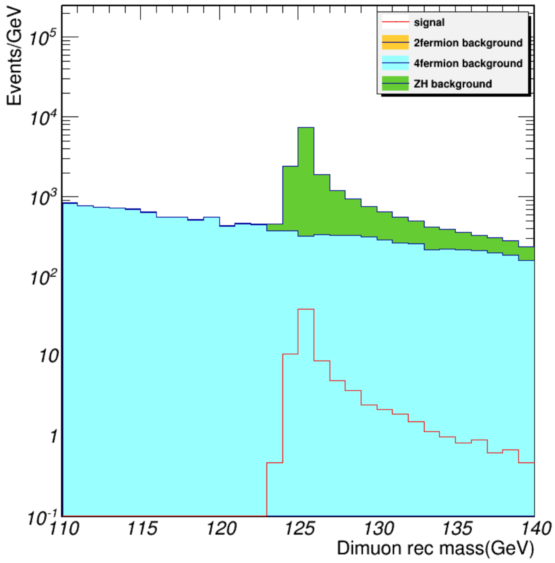

Figure 29: Distribution of the recoil mass of dimuon, after the previous cuts applied, before BDT decision applied.

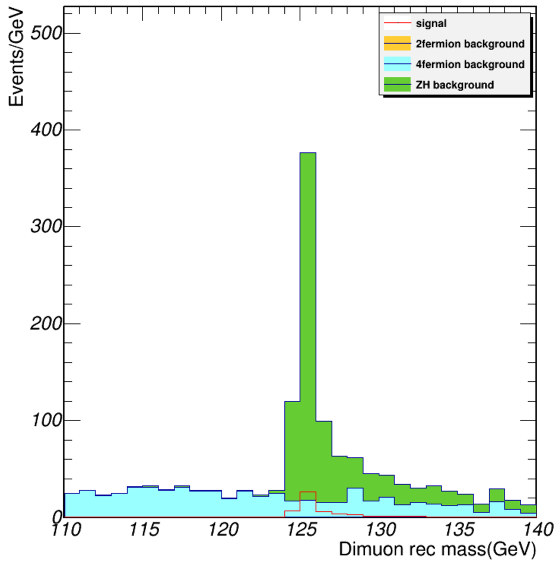

Figure 30: Distribution of the recoil mass of dimuon, after all of cuts & BDT decision applied.

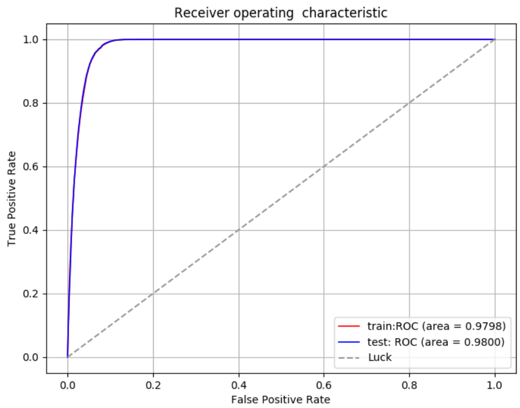

Figure 31: Receiver Operating Characteristic (ROC) curve.

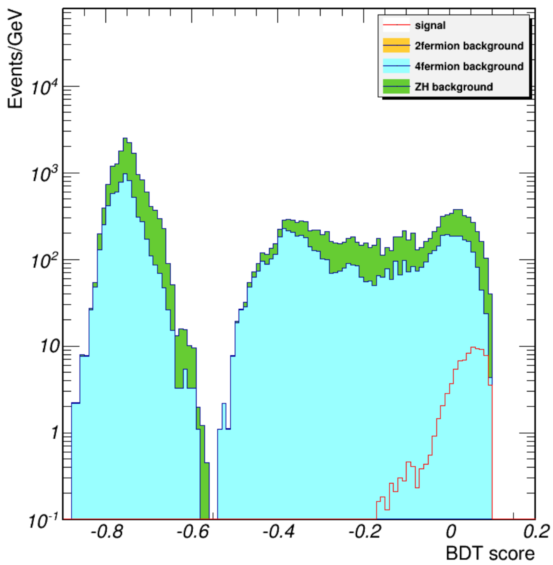

Figure 32: Classifier output distributions of signal and background.

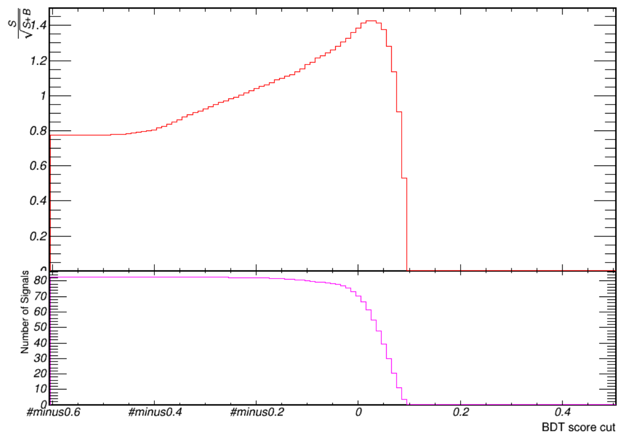

Figure 33: $\frac{S}{\sqrt{S+B}}$ vs BDT score curve.

5 Event Selection of Z(→$\nu\nu$)H(ZZ*→$\mu\mu qq$)

5.1 Z(→ $\nu\bar{\nu}$), H(ZZ*→$\mu^+\mu^-$→$q\bar{q}$)

5.1.1 Event selection (Cut-based only)

Table 15: Cut flow table for $\nu\nu\mu\mu qq$ channel

Cut	Signal	ZH Background	2f Background	4f Background	$\frac{S}{\sqrt{S+B}}$
$Expected$	6844.99±82.73	1140511±1067	801811977±28316	107203890±10353	
$Pre-selection$	238.62±15.45	30494 ±174	480828±693	515424±717	
$Signal\ or\ not$	226.71±15.06	30268 ±173	480828±693	515424±717	
$M_{dimuon} > M_{dijet}$	125.26±11.19	2832 ±53	421952±649	156993±396	0.1642
$N(pfo)$	117.12±10.82	1259 ±35	60398 ±245	68100 ±260	0.325
$M_{missing}$	102.67±10.13	147 ±12	2152 ±46	791 ±28	1.8168
M_{dimuon}	95.28 ±9.76	136 ±11	1762 ±41	258 ±16	2.007
M_{dijet}	94.12 ±9.7	131 ±11	258 ±16	204 ±14	3.5888
$*cos\ \theta$	94.12 ±9.7	131 ±11	258 ±16	204 ±14	3.5888
$cos\theta_{visible}$	89.46 ±9.46	125 ±11	37 ±6	57 ±7	5.0842
$Angle_{\mu j}$	83.85 ±9.16	72 ±8	0 ±0	16 ±4	6.3751
$*M^{rec}_{dimuon}$	83.85 ±9.16	72 ±8	0 ±0	16 ±4	6.3751
$*M^{rec}_{dijet}$	83.85 ±9.16	72 ±8	0 ±0	16 ±4	6.3751
$M_{visible}$	83.51 ±9.14	56 ±7	0 ±0	11 ±3	6.7871
$*P_{visible}$	83.51 ±9.14	56 ±7	0 ±0	11 ±3	6.7871
$*P_{T_{visible}}$	83.51 ±9.14	56 ±7	0 ±0	11 ±3	6.7871
$*E_{leading\ jet}$	83.51 ±9.14	56 ±7	0 ±0	11 ±3	6.7871
$*P_{T_{leading\ jet}}$	83.51 ±9.14	56 ±7	0 ±0	11 ±3	6.7871
$*E_{sub-leading\ jet}$	83.51 ±9.14	56 ±7	0 ±0	11 ±3	6.7871
$*P_{T_{sub-leading\ jet}}$	83.51 ±9.14	56 ±7	0 ±0	11 ±3	6.7871
$not\ \mu^+\mu^- HZZ$	72.56 ±8.52	17 ±4	0 ±0	9 ±3	7.2837
$not\ qqHZZ$	72.56 ±8.52	17 ±4	0 ±0	9 ±3	7.2837±0.5858

The event selection cuts are listed below in sequence.

- $M_{dimuon} > M_{dijets}$: the dimuon invariant mass is greater than the dijet invariant mass.

- $20 < N_{pfo} < 60$: Number of Prticle Flow Objects should be in this range.

- $75GeV < M^{Recoil}_{visible} < 110GeV$: the recoil mass of all visible particles should be in this range.

- $60GeV < M_{\mu^+\mu^-} < 100GeV$: the invariant mass of the dimuon should be in this range.

Table 16: Remained backgrounds (more than 1 event) after all of cuts applied.

name	scale	final
e2e2h_ww	0.08176	4
e2e2h_zz	0.010024	9
e3e3h_ww	0.0812	2
zz_sl0tau_up	1.10880522921	1
zz_l0taumu	1.0404004004	1
ww_sl0muq	1.10890944134	3
ww_sl0tauq	1.10899434445	1
zzorww_l0mumu	1.10891486372	1
sze_l0mu	1.10916641266	1

Table 17: Remained backgrounds (more than 1 event) before final two cuts applied.

name	scale	final
e2e2h_e3e3	0.023968	1
e2e2h_ww	0.08176	13
e2e2h_zz	0.010024	39
e3e3h_ww	0.0812	2
zz_sl0tau_up	1.10880522921	2
zz_l0taumu	1.0404004004	2
ww_sl0muq	1.10890944134	3
ww_sl0tauq	1.10899434445	1
zzorww_l0mumu	1.10891486372	1
sze_l0mu	1.10916641266	1

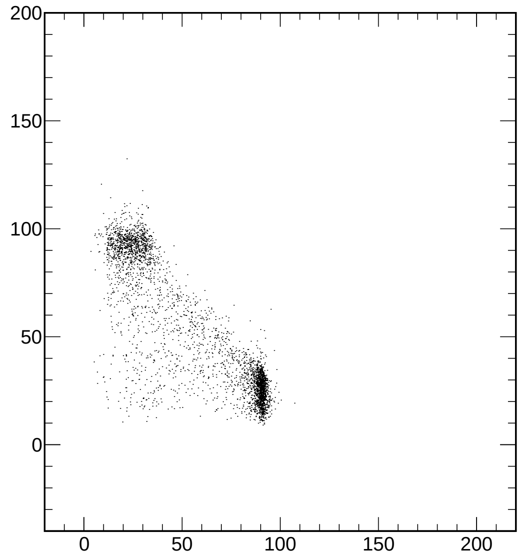

Figure 34: dimuon invariant mass vs dijet invariant mass.

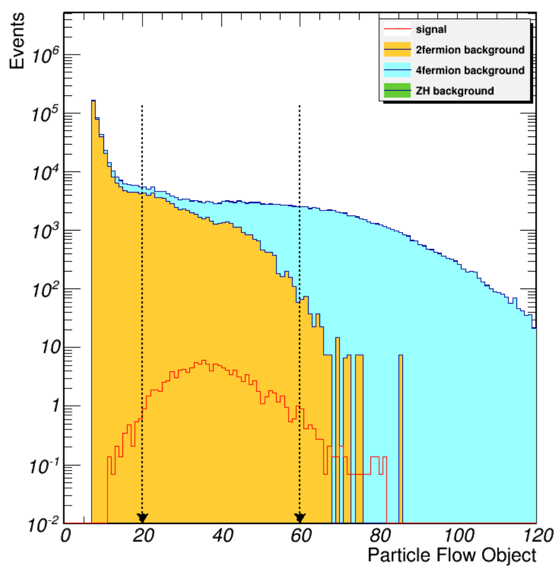

Figure 35: Number of PFOs.

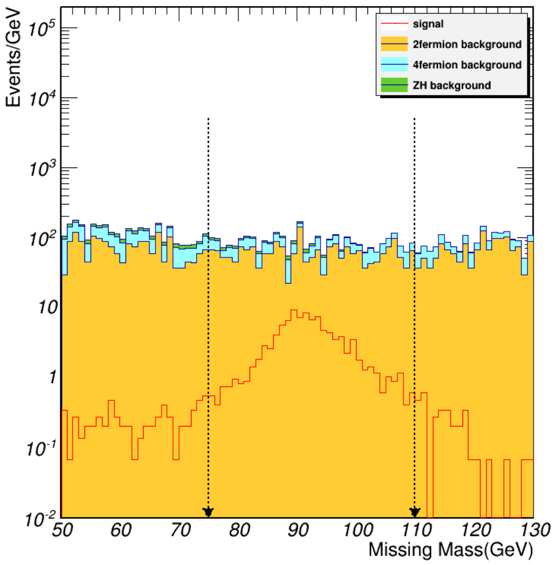

Figure 36: Recoil mass of visible particles.

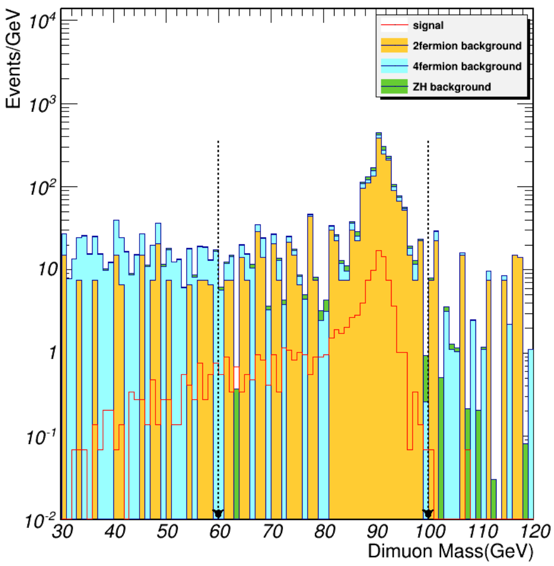

Figure 37: Invariant mass of di-muons.

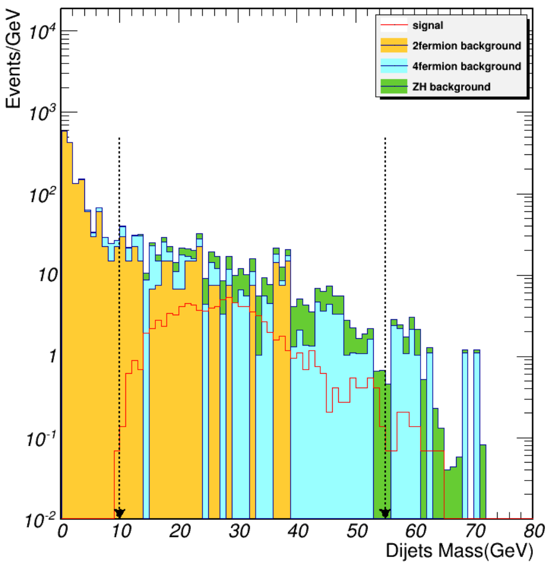

Figure 38: Invariant mass of di-jets.

- $10GeV < M_{dijet} < 55GeV$: the invariant mass of dijet should be in this range.

- $-0.95 < cos\ \theta_{visible} < 0.95$: $cos\theta$ of the summation of all visible particles should be in this range.

- $Min\ angle\ <\ 135°$: Minimum angle between the two Z(Z*) reconstructed by leptons and jets should be within this range .

- $110GeV < M_{visible} < 140GeV$: the invariant mass of all visible particles should be in this range.

Two additional cuts:

- $M^{rec}_{dimuon} < 122GeV\ or\ M^{rec}_{dimuon} > 128GeV$: To avoid the overlap events with $\mu\mu$HZZ signals.
- $M^{rec}_{dijet} < 122GeV\ or\ M^{rec}_{dijet} > 128GeV$: To remove the overlap events with qqHZZ signals.

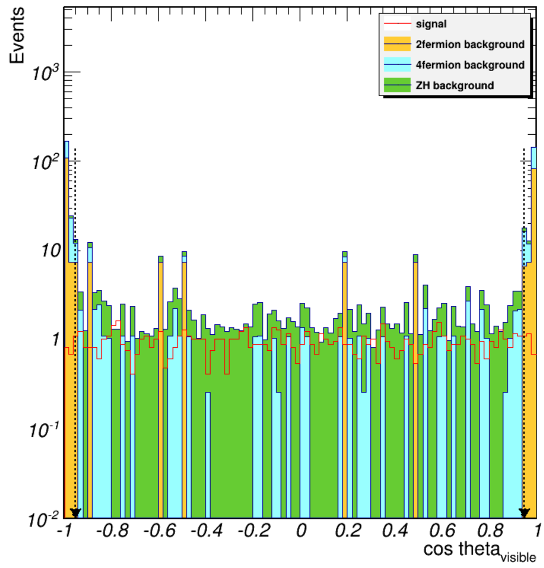

Figure 39: All visible particle $cos\ \theta$

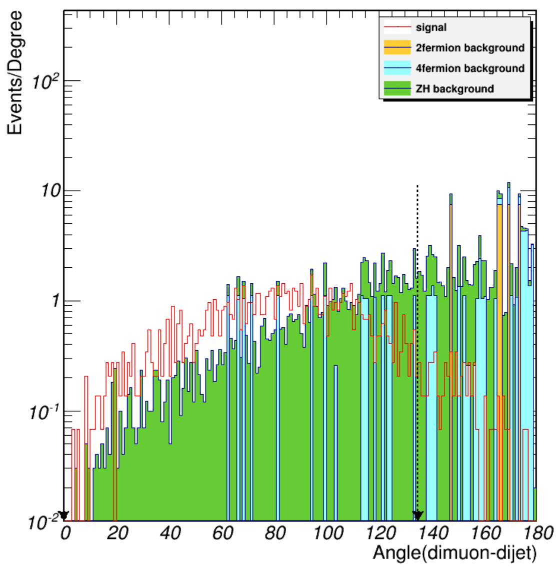

Figure 40: Minimum angle between the two Z(Z*) reconstructed by leptons and jets.

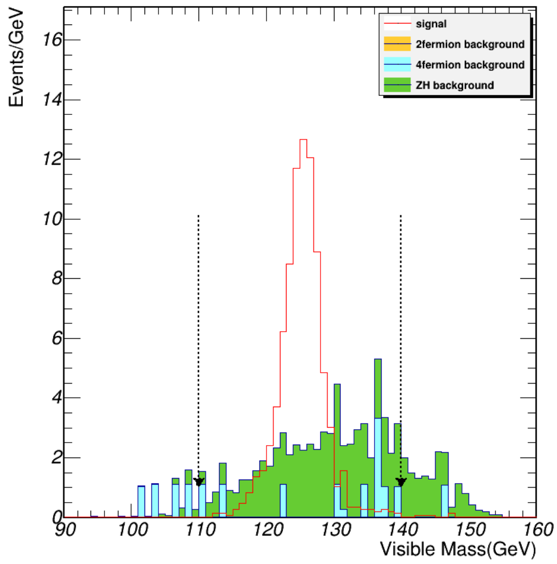

Figure 41: Invariant mass of all visible particles.

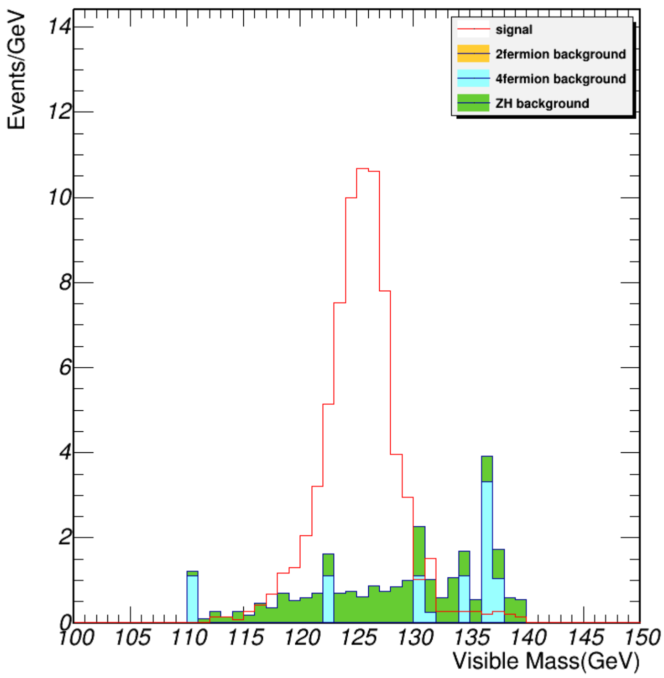

Figure 42: Distribution of the visible mass of all particles, after all of cuts applied.

5.1.2 Event selection combined with BDT method

Table 18: Cut flow table for $\nu\nu\mu\mu qq$ channel with BDT

Cut	Signal	ZH Background	2f Background	4f Background	$\frac{S}{\sqrt{S+B}}$
$Expected$	6844	1140511	801811977	107203890	
$Pre-selection$	238	30494	480828	515424	
$Signal\ or\ not$	226	30268	480828	515424	
$M_{dimuon} > M_{dijet}$	125	2832	421952	156993	0.1642
$N(pfo)$	117	1259	60398	68100	0.325
$M_{missing}$	102	147	2152	791	1.8168
$M_{visible}$	101	82	696	325	2.9267
$cos\theta_{visible}$	96	77	124	79	4.9672
$BDT\ score$	80	12	0	27	7.383

- $M_{dimuon} > M_{dijet}$: the dimuon invariant mass is greater than the dijet invariant mass.
- $20 < N_{pfo} < 60$: Number of PFO is greater than 20 and less than 60.
- $75GeV < M_{missing} < 110GeV$: the missing mass should be in this range.
- $110GeV < M_{visible} < 140GeV$: the invariant mass of the summation of all visible particles should be in this range.
- $-0.95 < cos\ \theta_{visible} < 0.95$: $cos\theta$ of the summation of all visible particles should be in this range.
- $BDT\ score > -0.01$: BDT score greater than 0.15.

Table 19: Remained backgrounds (more than 1 event) after all of cuts applied.

name	scale	final
e2e2h_ww	0.08176	3
e2e2h_zz	0.010024	4
e3e3h_ww	0.0812	2
zz_sl0tau_up	1.10880522921	4
zz_l0taumu	1.0404004004	3
ww_sl0muq	1.10890944134	9
ww_sl0tauq	1.10899434445	4
zzorww_l0mumu	1.10891486372	3
sze_l0mu	1.10916641266	1

The input variable list is: M_{dimuon}, M_{dijet}, $M_{missing}$, N_{pfo}, $cos\ \theta$, $cos\ \theta_{visible}$, $Angle_{\mu^+\mu^- - dijet}$, M^{rec}_{dijet}, M^{rec}_{dimuon}, $P_{visible}$, $P_{T_{visible}}$, $E_{leading\ \ jet}$, $P_{T_{leading\ \ jet}}$, $E_{sub-leading\ \ jet}$, $P_{T_{sub-leading\ \ jet}}$. All the variables that are used in cut-based study are in the input variable list for BDT, except $M_{visible}$, since it is the final observable.

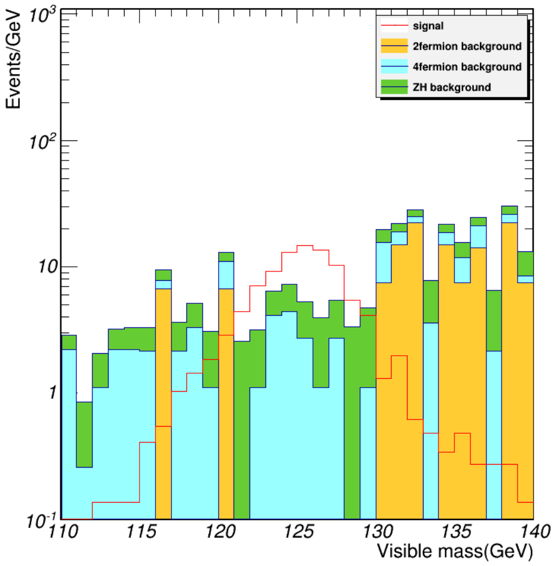

Figure 43: Distribution of the visible mass, after the previous cuts applied, before BDT decision applied.

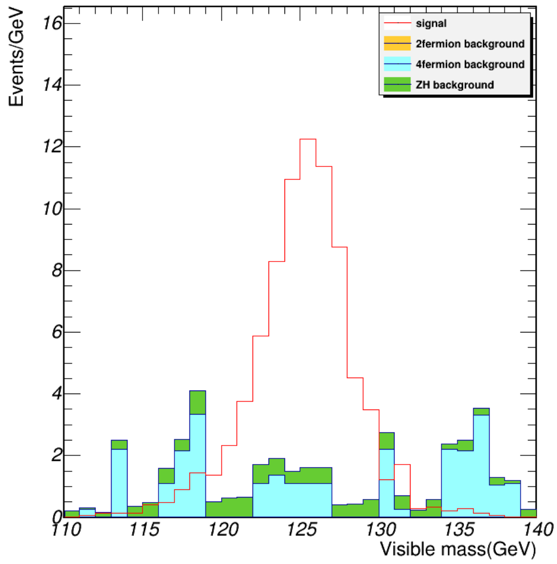

Figure 44: Distribution of the visible mass, after all of cuts & BDT decision applied.

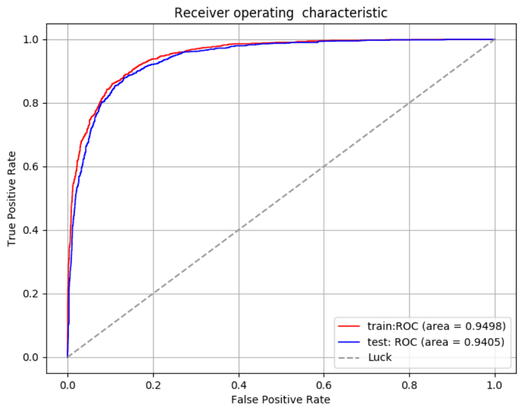

Figure 45: Receiver Operating Characteristic (ROC) curve.

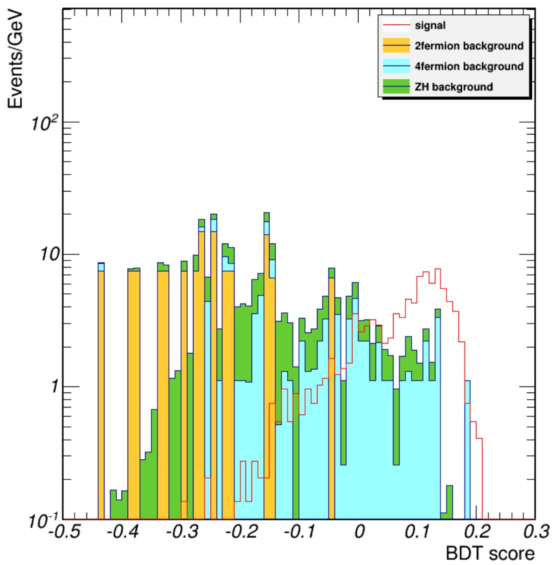

Figure 46: Classifier output distributions of signal and background.

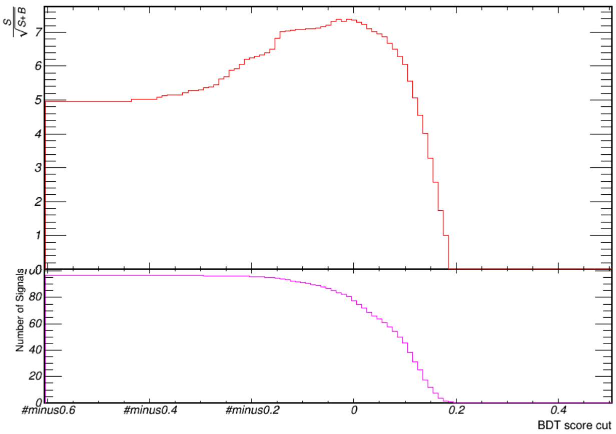

Figure 47: $\frac{S}{\sqrt{S+B}}$ vs BDT score curve.

5.2 Z($\to \nu\bar{\nu}$), H(Z$\to q\bar{q}$, Z*$\to \mu^+\mu^-$)

5.2.1 Event selection (Cut-based only)

The event selection cuts are listed below in sequence.

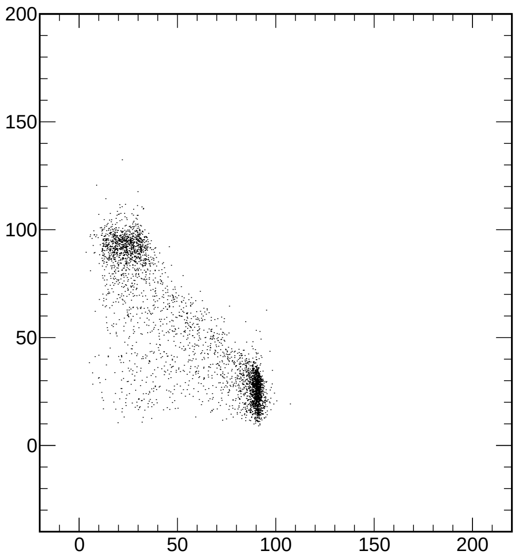

Figure 48: dimuon invariant mass vs dijet invariant mass.

- $M_{dimuon} < M_{dijets}$: the dijet invariant mass is greater than the dimuon invariant mass.

- $30 < N_{pfo} < 100$: Number of Prticle Flow Objects should be in this range.

Table 20: Cut flow table for $\nu\nu qq\mu\mu$ channel

Cut	Signal	ZH Background	2f Background	4f Background	$\frac{S}{\sqrt{S+B}}$
$Expected$	6844.99±82.73	1140511±1067	801811977±28316	107203890±10353	
$Pre-selection$	238.62±15.45	30494 ±174	480828±693	515424±717	
$Signal\ or\ not$	226.71±15.06	30268 ±173	480828±693	515424±717	
$M_{dimuon} < M_{dijet}$	101.44±10.07	27436 ±165	58876 ±242	358431±598	0.1521
$N(pfo)$	97.54 ±9.88	20843 ±144	364 ±19	231698±481	0.1939
$M_{missing}$	79.06 ±8.89	769 ±27	37 ±6	2083 ±45	1.4508
M_{dimuon}	78.38 ±8.85	707 ±26	7 ±2	1732 ±41	1.5596
M_{dijet}	68.04 ±8.25	576 ±24	0 ±0	830 ±28	1.7719
$*cos\ \theta$	68.04 ±8.25	576 ±24	0 ±0	830 ±28	1.7719
$cos\theta_{visible}$	64.55 ±8.03	552 ±23	0 ±0	452 ±21	1.9743
$Angle_{\mu j}$	60.65 ±7.79	269 ±16	0 ±0	78 ±8	2.9985
$*M^{rec}_{dimuon}$	60.65 ±7.79	269 ±16	0 ±0	78 ±8	2.9985
$*M^{rec}_{dijet}$	60.65 ±7.79	269 ±16	0 ±0	78 ±8	2.9985
$M_{visible}$	59.89 ±7.74	211 ±14	0 ±0	65 ±8	3.2662
$*P_{visible}$	59.89 ±7.74	211 ±14	0 ±0	65 ±8	3.2662
$*P_{T_{visible}}$	59.89 ±7.74	211 ±14	0 ±0	65 ±8	3.2662
$*E_{leading\ jet}$	59.89 ±7.74	211 ±14	0 ±0	65 ±8	3.2662
$*P_{T_{leading\ jet}}$	59.89 ±7.74	211 ±14	0 ±0	65 ±8	3.2662
$*E_{sub-leading\ jet}$	59.89 ±7.74	211 ±14	0 ±0	65 ±8	3.2662
$*P_{T_{sub-leading\ jet}}$	59.89 ±7.74	211 ±14	0 ±0	65 ±8	3.2662
$not\ \mu^+\mu^- HZZ$	59.89 ±7.74	211 ±14	0 ±0	65 ±8	3.2662
$not\ qqHZZ$	52.3 ±7.23	159 ±12	0 ±0	52 ±7	3.2227±0.4654

Table 21: Remained backgrounds (more than 1 event) after all of cuts applied.

name	scale	final
e2e2h_bb	0.21896	8
e2e2h_ww	0.08176	7
e3e3h_bb	0.21784	3
e3e3h_ww	0.0812	11
qqh_e3e3	0.4844	50
qqh_ww	1.6464	55
qqh_zz	0.20216	18
zz_sl0mu_down	1.08025726079	3
zz_sl0tau_up	1.10880522921	9
zz_sl0tau_down	1.10887174477	25
ww_sl0muq	1.10890944134	2
ww_sl0tauq	1.10899434445	4
sze_l0mu	1.10916641266	6

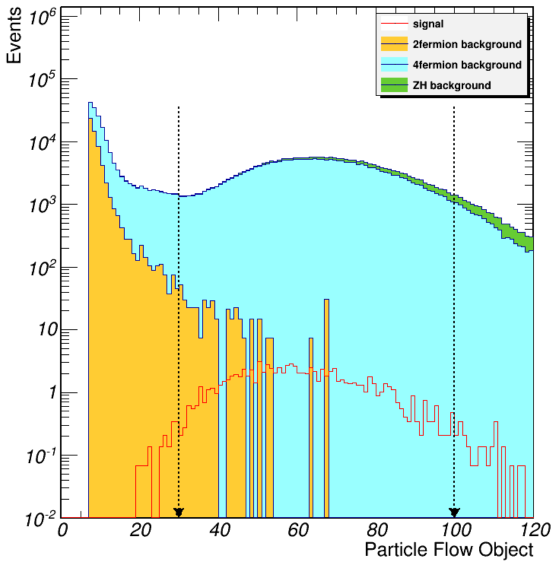

Figure 49: Number of PFOs.

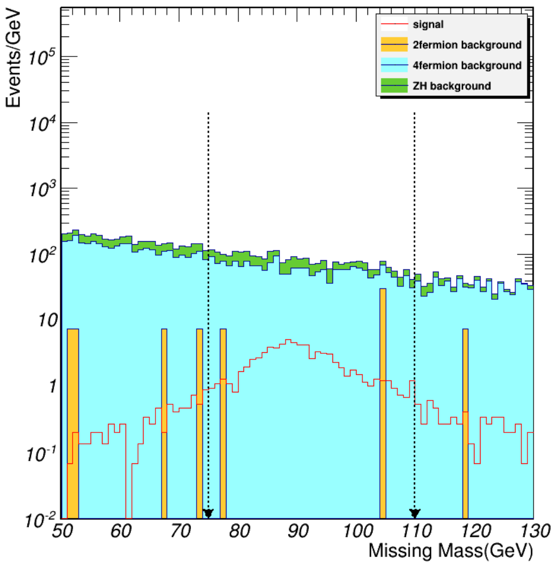

Figure 50: Recoil mass of visible particles.

- $75GeV < M^{Recoil}_{visible} < 110GeV$: the recoil mass of all visible particles should be in this range.

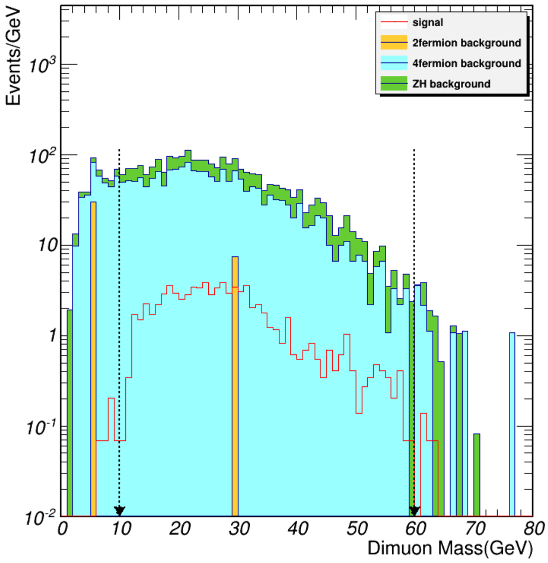

Figure 51: Invariant mass of di-muons.

- $10GeV < M_{\mu^+\mu^-} < 60GeV$: the invariant mass of the dimuon should be in this range.

- $60GeV < M_{dijet} < 100GeV$: the invariant mass of dijet should be in this range.

- $-0.95 < cos\ \theta_{visible} < 0.95$: $cos\theta$ of the summation of all visible particles should be in this range.

- $Min\ angle\ <\ 135°$: Minimum angle between the two Z(Z*) reconstructed by leptons and jets should be within this range .

- $110GeV < M_{visible} < 140GeV$: the invariant mass of all visible particles should be in this range.

Two additional cuts:

- $M^{rec}_{dimuon} < 122GeV\ or\ M^{rec}_{dimuon} > 128GeV$: To avoid the overlap events with $\mu\mu$HZZ signals.
- $M^{rec}_{dijet} < 122GeV\ or\ M^{rec}_{dijet} > 128GeV$: To remove the overlap events with qqHZZ signals.

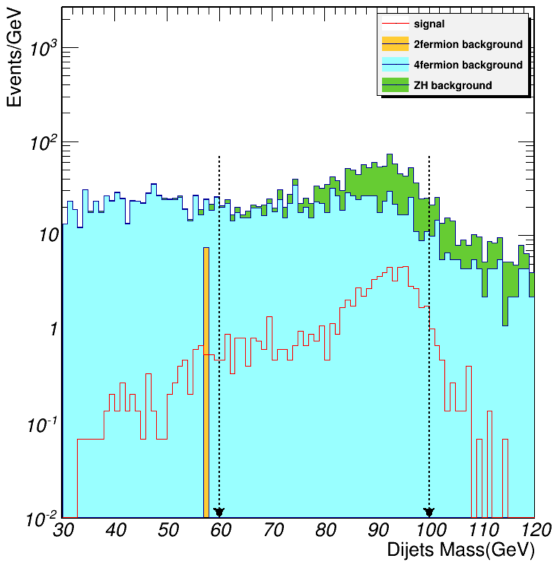

Figure 52: Invariant mass of di-jets.

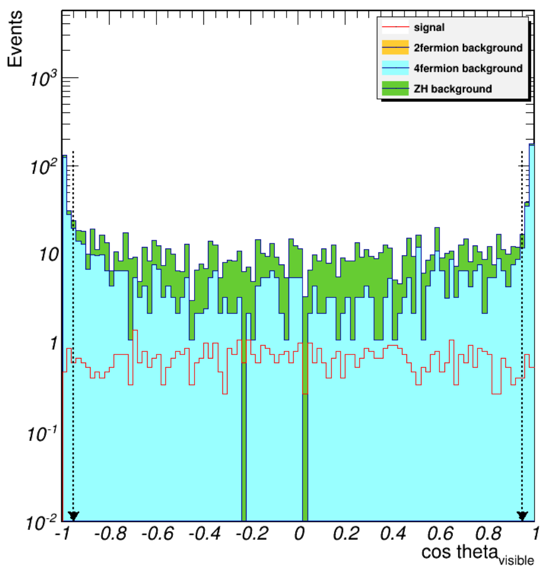

Figure 53: All visible particle $cos\ \theta$

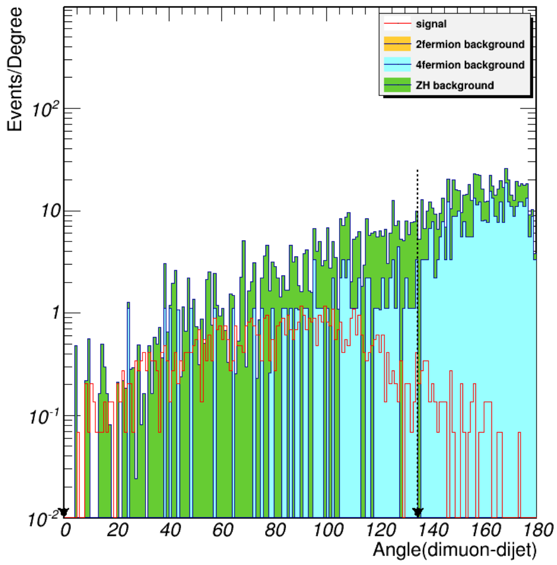

Figure 54: Minimum angle between the two Z(Z*) reconstructed by leptons and jets.

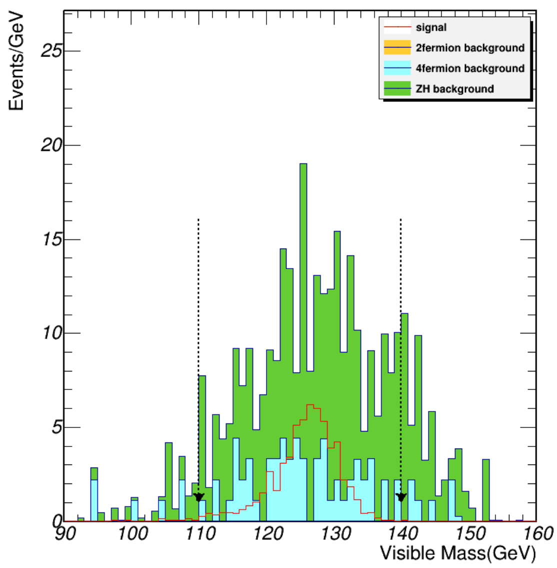

Figure 55: Invariant mass of all visible particles.

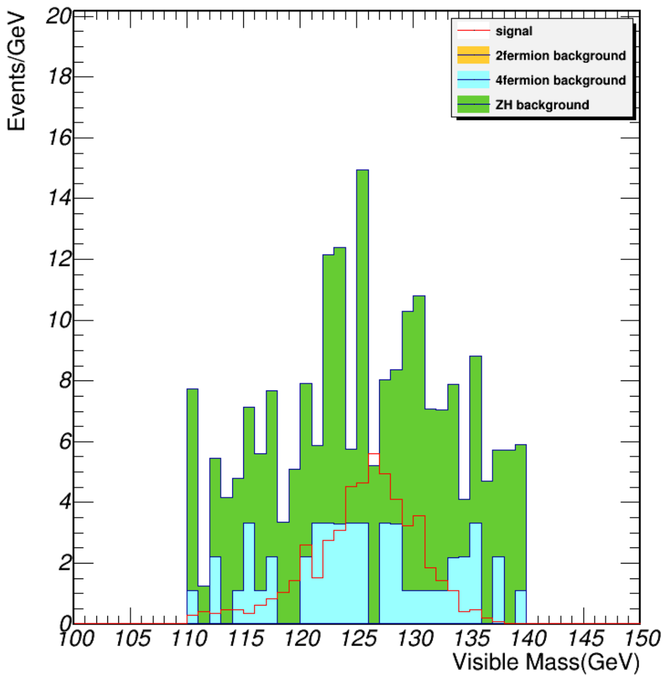

Figure 56: Distribution of the visible mass of all particles, after all of cuts applied.

5.2.2 Event selection combined with BDT method

- $M_{dimuon} < M_{dijet}$: the dimuon invariant mass is smaller than the dijet invariant mass.
- $30 < N_{pfo} < 100$: Number of PFO is greater than 30 and less than 100.
- $75GeV < M_{missing} < 110GeV$: the missing mass should be in this range.
- $110GeV < M_{visible} < 140GeV$: the invariant mass of the summation of all visible particles should be in this range.
- $-0.95 < cos\ \theta_{visible} < 0.95$: $cos\theta$ of the summation of all visible particles should be in this range.
- $BDT\ \ score > 0$: BDT score greater than 0.

The input variable list is: M_{dimuon}, M_{dijet}, $M_{missing}$, N_{pfo}, $cos\ \theta$, $cos\ \theta_{visible}$, $Angle_{\mu^+\mu^- - dijet}$, M^{rec}_{dijet}, M^{rec}_{dimuon}, $P_{visible}$, $P_{T_{visible}}$, $E_{leading\ \ jet}$, $P_{T_{leading\ \ jet}}$, $E_{sub-leading\ \ jet}$, $P_{T_{sub-leading\ \ jet}}$. All the variables that are used in cut-based study are in the input variable list for BDT, except $M_{visible}$, since it is the final observable.

Table 22: Cut flow table for $\nu\nu qq\mu\mu$ channel with BDT

Cut	Signal	ZH Background	2f Background	4f Background	$\frac{S}{\sqrt{S+B}}$
$Expected$	6844	1140511	801811977	107203890	
$Pre-selection$	238	30494	480828	515424	
$Signal\ or\ not$	226	30268	480828	515424	
$M_{dimuon} < M_{dijet}$	101	27436	58876	358431	0.1521
$N(pfo)$	97	20843	364	231698	0.1939
$M_{missing}$	79	769	37	2083	1.4508
$M_{visible}$	76	445	0	910	2.0327
$cos\theta_{visible}$	73	430	0	360	2.4836
$BDT\ score$	47	76	0	16	3.9875

Table 23: Remained backgrounds (more than 1 event) after all of cuts applied.

name	scale	final
e2e2h_bb	0.21896	4
e2e2h_ww	0.08176	4
e3e3h_ww	0.0812	3
qqh_e3e3	0.4844	21
qqh_ww	1.6464	29
qqh_zz	0.20216	11
zz_sl0mu_down	1.08025726079	2
zz_sl0tau_up	1.10880522921	1
zz_sl0tau_down	1.10887174477	7
ww_sl0muq	1.10890944134	4
ww_sl0tauq	1.10899434445	1

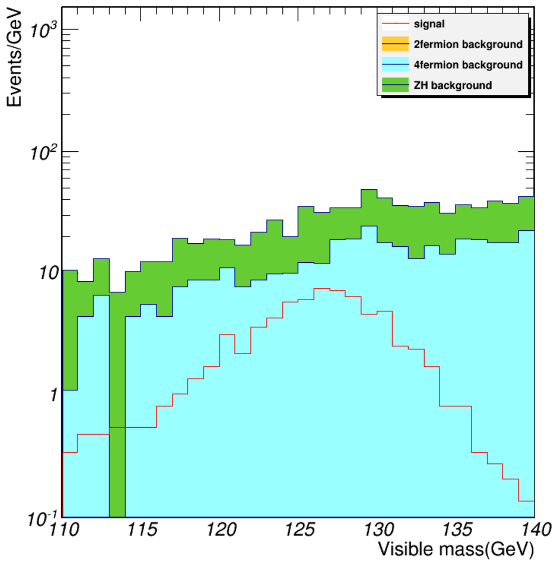

Figure 57: Distribution of the visible mass, after the previous cuts applied, before BDT decision applied.

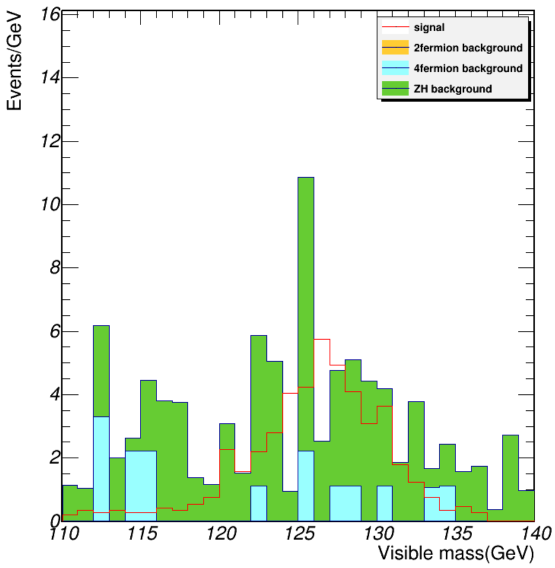

Figure 58: Distribution of the visible mass, after all of cuts & BDT decision applied.

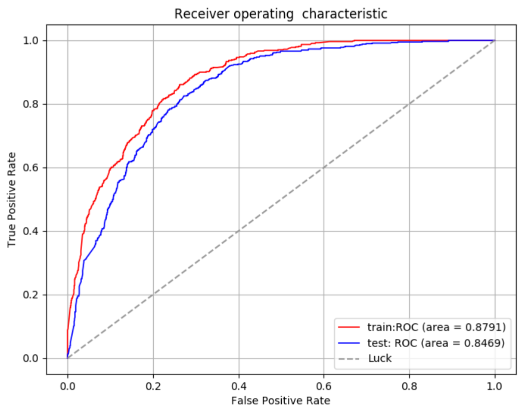

Figure 59: Receiver Operating Characteristic (ROC) curve.

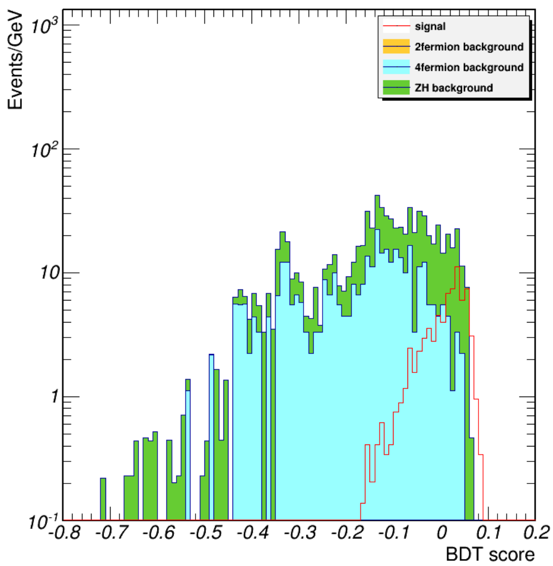

Figure 60: Classifier output distributions of signal and background.

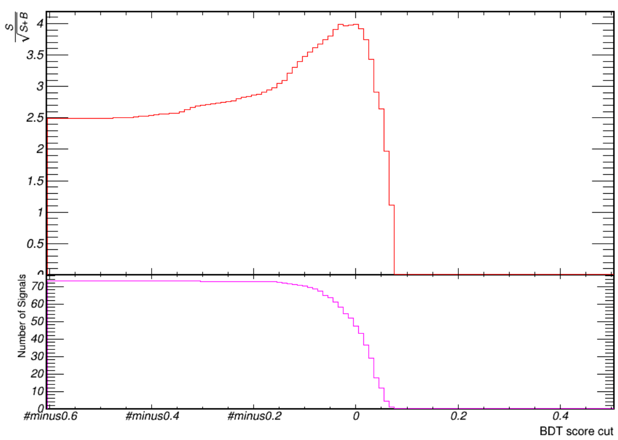

Figure 61: $\frac{S}{\sqrt{S+B}}$ vs BDT score curve.

6 Event Selection of Z($\rightarrow qq$)H(ZZ*$\rightarrow \nu\nu\mu\mu$)

6.1 Z($\rightarrow q\bar{q}$), H(Z$\rightarrow \nu\bar{\nu}$,Z*$\rightarrow \mu^{+}\mu^{-}$)

6.1.1 Event selection (Cut-based only)

Table 24: Cut flow table for $qq\nu\nu\mu\mu$ channel

Cut	Signal	ZH Background	2f Background	4f Background	$\frac{S}{\sqrt{S+B}}$
$Expected$	20254.08±142.32	1140511±1067	801811977±28316	107203890±10353	
$Pre-selection$	826.57±28.75	30494 ±174	480828±693	515424±717	
$Signal\ or\ not$	203.35±14.26	30291 ±174	480828±693	515424±717	
$M_{missing} > M_{dimuon}$	94.99 ±9.75	3179 ±56	18606 ±136	40769 ±201	0.3795
$N(pfo)$	84.66 ±9.2	2242 ±47	1212 ±34	12626 ±112	0.6659
M_{dijet}	75.14 ±8.67	1532 ±39	7 ±2	4965 ±70	0.9263
M_{dimuon}	68.05 ±8.25	1231 ±35	0 ±0	2803 ±52	1.0623
$M_{missing}$	57.72 ±7.6	575 ±23	0 ±0	572 ±23	1.6625
$*cos\ \theta$	57.72 ±7.6	575 ±23	0 ±0	572 ±23	1.6625
$cos\theta_{visible}$	55.09 ±7.42	551 ±23	0 ±0	403 ±20	1.7334
$*Angle_{\mu j}$	55.09 ±7.42	551 ±23	0 ±0	403 ±20	1.7334
M^{rec}_{dimuon}	53.47 ±7.31	493 ±22	0 ±0	348 ±18	1.7877
M^{rec}_{dijet}	51.24 ±7.16	418 ±20	0 ±0	237 ±15	1.9265
$M_{visible}$	48.0 ±6.93	374 ±19	0 ±0	209 ±14	1.9087
$*P_{visible}$	48.0 ±6.93	374 ±19	0 ±0	209 ±14	1.9087
$*P_{T_{visible}}$	48.0 ±6.93	374 ±19	0 ±0	209 ±14	1.9087
$*E_{leading\ jet}$	48.0 ±6.93	374 ±19	0 ±0	209 ±14	1.9087
$*P_{T_{leading\ jet}}$	48.0 ±6.93	374 ±19	0 ±0	209 ±14	1.9087
$*E_{sub-leading\ jet}$	48.0 ±6.93	374 ±19	0 ±0	209 ±14	1.9087
$*P_{T_{sub-leading\ jet}}$	48.0 ±6.93	374 ±19	0 ±0	209 ±14	1.9087
$not\ \mu^{+}\mu^{-}HZZ$	48.0 ±6.93	374 ±19	0 ±0	209 ±14	1.9087
$not\ \nu\nu HZZ$	41.72 ±6.46	326 ±18	0 ±0	190 ±13	1.764 ±0.3625

The event selection cuts are listed below in sequence.

- $M_{miss} > M_{dimuon}$: the missing mass is greater than the dimuon invariant mass.

- $40 < N_{pfo} < 95$: Number of Prticle Flow Objects should be in this range.

- $75GeV < M_{dijet} < 105GeV$: the invariant mass of dijet should be in this range.

- $15GeV < M_{\mu^{+}\mu^{-}} < 55GeV$: the invariant mass of the dimuon should be in this range.

Table 25: Remained backgrounds (more than 1 event) after all of cuts applied.

name	scale	final
e2e2h_bb	0.21896	12
e2e2h_ww	0.08176	4
e3e3h_bb	0.21784	8
e3e3h_ww	0.0812	10
nnh_zz	0.06832	18
qqh_e3e3	0.4844	182
qqh_ww	1.6464	87
zz_sl0mu_up	1.09032214858	4
zz_sl0mu_down	1.08025726079	5
zz_sl0tau_up	1.10880522921	58
zz_sl0tau_down	1.10887174477	115
sze_l0mu	1.10916641266	6

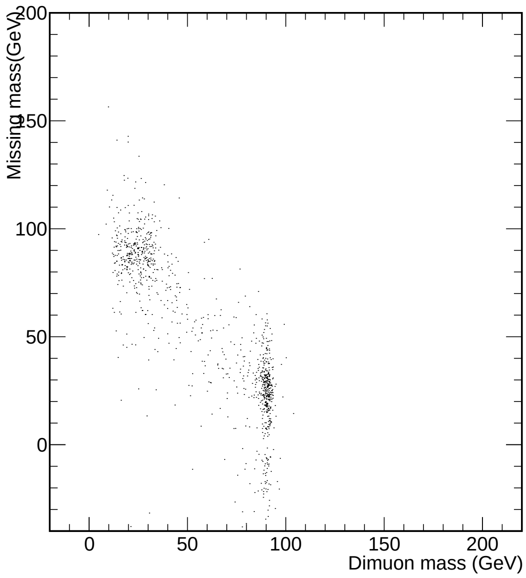

Figure 62: Missing mass vs dimuon invariant mass.

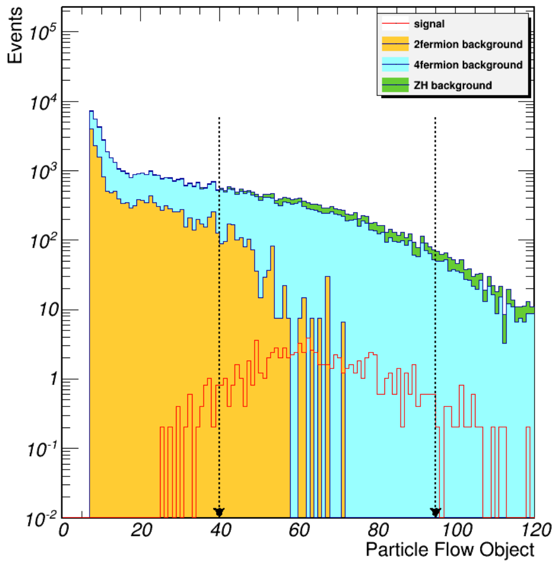

Figure 63: Number of PFOs.

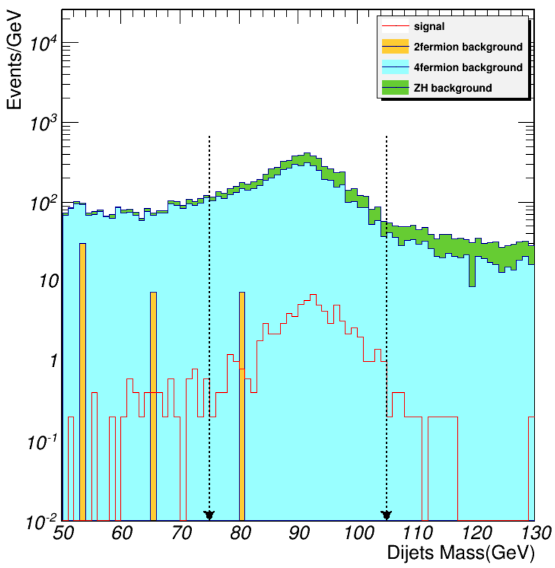

Figure 64: Invariant mass of di-jets.

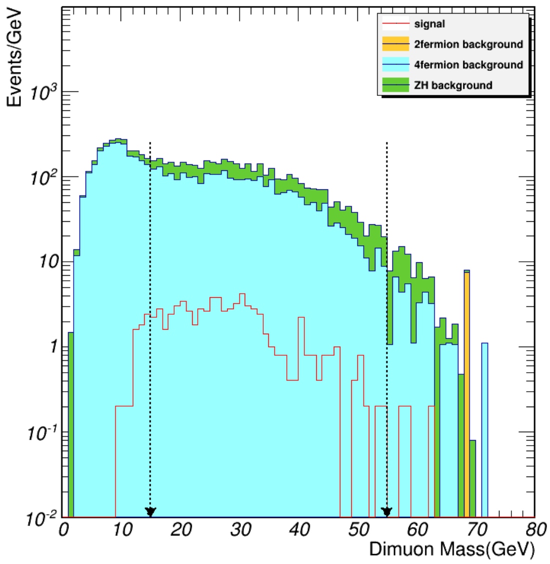

Figure 65: Invariant mass of di-muons.

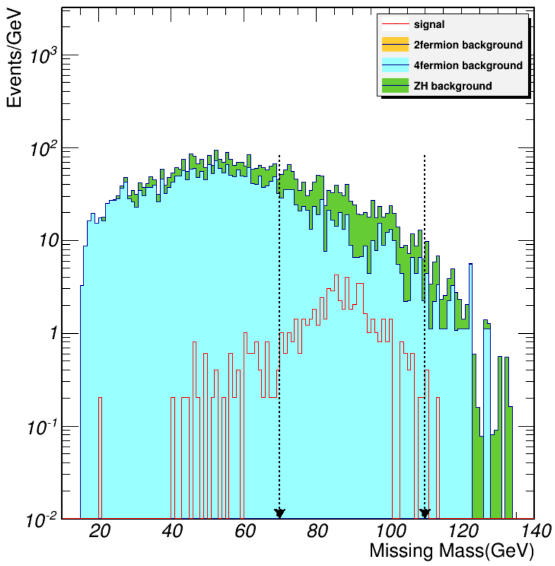

Figure 66: Recoil mass of visible particles.

- $70GeV < M^{Recoil}_{visible} < 110GeV$: the recoil mass of all visible particles should be in this range.

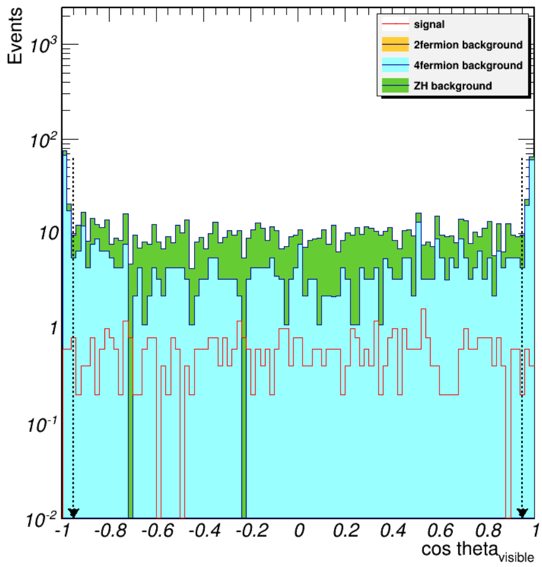

Figure 67: All visible particle $cos\ \theta$

- $-0.95 < cos\ \theta_{visible} < 0.95$: $cos\theta$ of the summation of all visible particles should be in this range.

- $175GeV < M^{dimuon}_{Recoil} < 215GeV$: the recoil mass of the dimuon should be in this range.

- $110GeV < M^{dijet}_{Recoil} < 140GeV$: the recoil mass of the dijet should be in this range.

- $115GeV < M_{visible} < 155GeV$: the visible mass of all particles should be in this range.

Two additional cuts:

- $M^{rec}_{dimuon} < 122GeV\ or\ M^{rec}_{dimuon} > 128GeV$: To avoid the overlap events with $\mu\mu$HZZ signals.

- $M_{visible} < 122GeV\ or\ M_{visible} > 128GeV$: To remove the overlap events with $\nu\nu$HZZ signals.

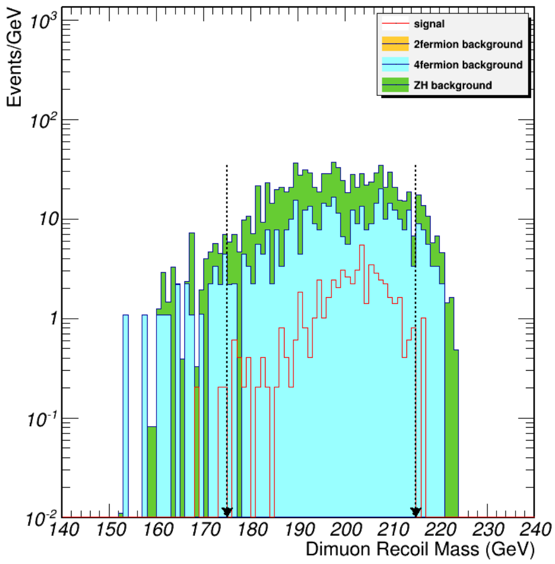

Figure 68: Recoil mass of di-muons.

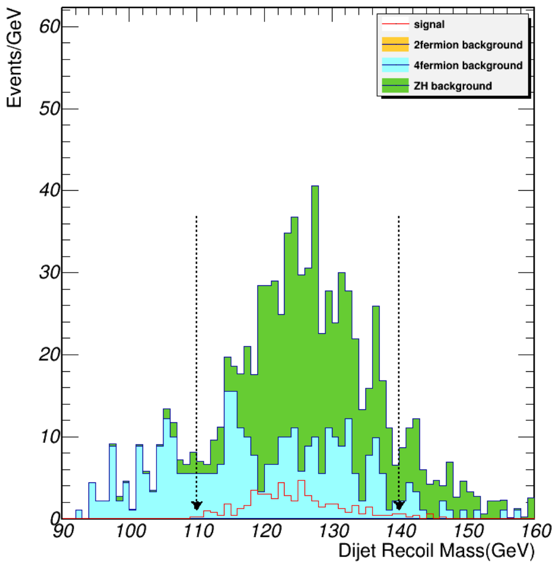

Figure 69: Recoil mass of di-jets.

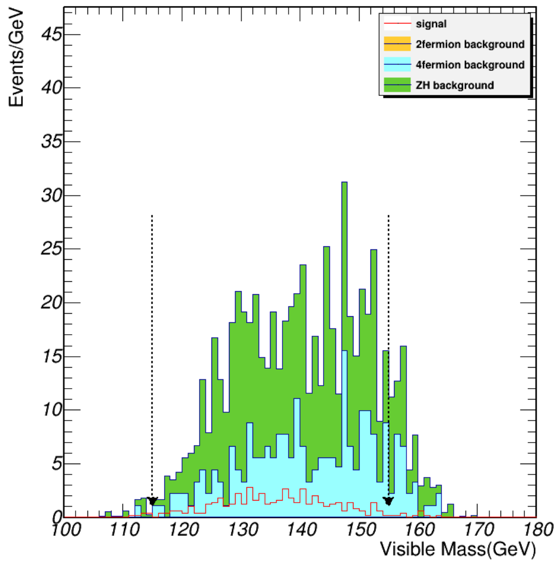

Figure 70: Visible mass of all particles.

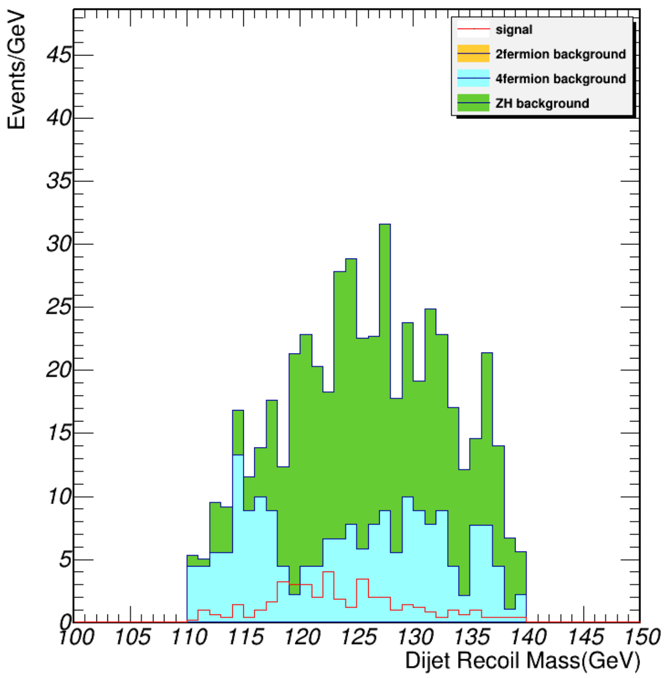

Figure 71: Distribution of the recoil mass of dijet, after all of cuts applied.

6.1.2 Event selection combined with BDT method

Table 26: Cut flow table for $qq\nu\nu\mu\mu$ channel with BDT

Cut	Signal	ZH Background	2f Background	4f Background	$\frac{S}{\sqrt{S+B}}$
$Expected$	20254	1140511	801811977	107203890	
$Pre-selection$	826	30494	480828	515424	
$Signal\ or\ not$	203	30291	480828	515424	
$M_{missing} > M_{dimuon}$	94	3179	18606	40769	0.3795
$N(pfo)$	84	2242	1212	12626	0.6659
M_{dijet}	75	1532	7	4965	0.9263
M^{rec}_{dijet}	70	1318	0	1381	1.3315
$cos\theta_{visible}$	67	1259	0	541	1.551
$BDT\ score$	48	305	0	116	2.2226

- $M_{missing} > M_{dimuon}$: the missing mass is greater than the dimuon invariant mass.
- $40 < N_{pfo} < 95$: Number of PFO is greater than 40 and less than 95.
- $75GeV < M_{dijet} < 105GeV$: the invariant mass of dijet should be in this range.
- $110GeV < M^{rec}_{dijet} < 140GeV$: the recoil mass of the dijet should be in this range.
- $-0.95 < cos\ \theta_{visible} < 0.95$: $cos\theta$ of the summation of all visible particles should be in this range.
- $BDT\ score > -0.05$: BDT score greater than -0.05.

Table 27: Remained backgrounds (more than 5 event) after all of cuts applied.

name	scale	final
e2e2h_bb	0.21896	6
e3e3h_bb	0.21784	6
e3e3h_ww	0.0812	6
nnh_zz	0.06832	24
qqh_e3e3	0.4844	151
qqh_ww	1.6464	107
zz_sl0tau_up	1.10880522921	36
zz_sl0tau_down	1.10887174477	76

The input variable list is: M_{dimuon}, M_{dijet}, $M_{missing}$, N_{pfo}, $cos\ \theta$, $cos\ \theta_{visible}$, $Angle_{\mu^+\mu^- - dijet}$, M^{rec}_{dimuon}, $M_{visible}$, $P_{visible}$, $P_{T_{visible}}$, $E_{leading\ jet}$, $P_{T_{leading\ jet}}$, $E_{sub-leading\ jet}$, $P_{T_{sub-leading\ jet}}$. All the variables that are used in cut-based study are in the input variable list for BDT, except M^{rec}_{dijet}, since it is the final observable.

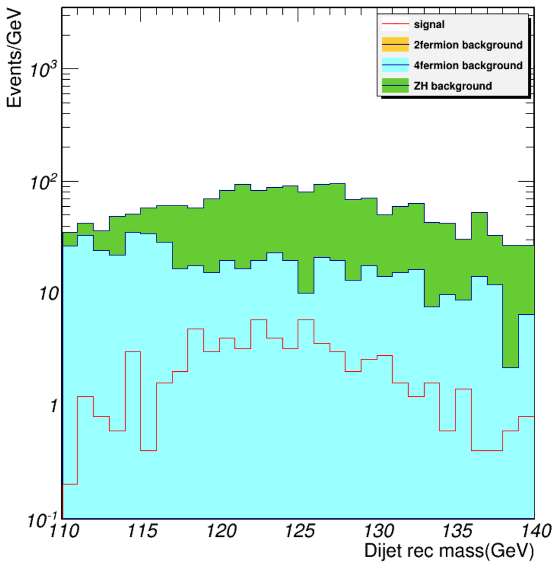

Figure 72: Distribution of the recoil mass of dijet, after the previous cuts applied, before BDT decision applied.

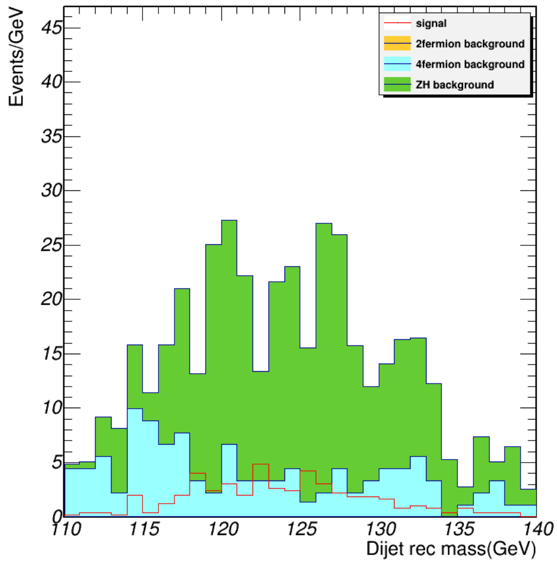

Figure 73: Distribution of the recoil mass of dijet, after all of cuts & BDT decision applied.

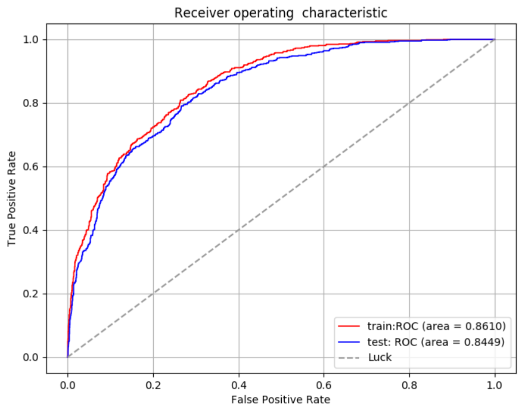

Figure 74: Receiver Operating Characteristic (ROC) curve.

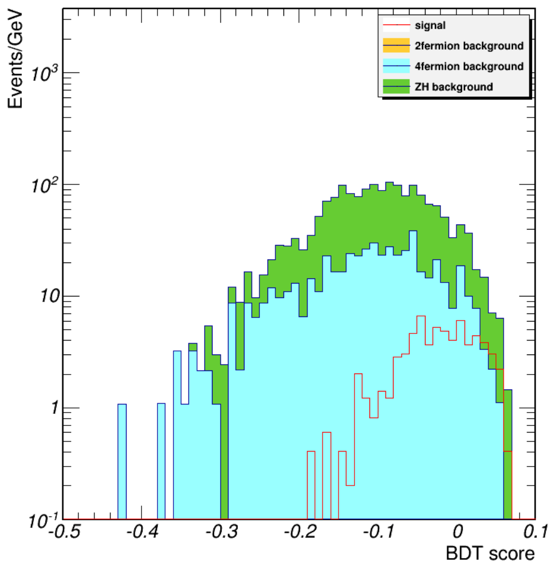

Figure 75: Classifier output distributions of signal and background.

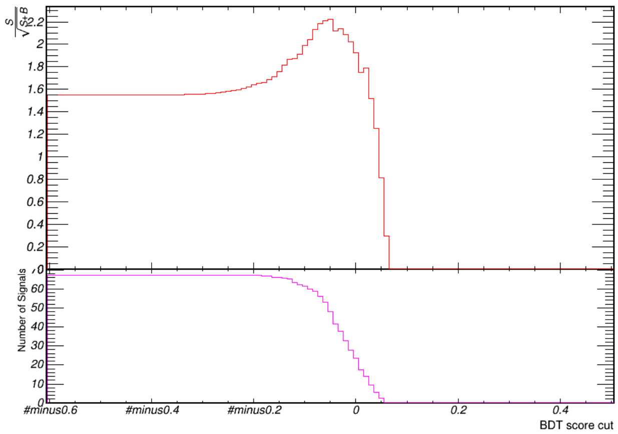

Figure 76: $\frac{S}{\sqrt{S+B}}$ vs BDT score curve.

6.2 Z($\rightarrow q\bar{q}$), H(Z$\rightarrow\mu^{+}\mu^{-}$, Z*$\rightarrow\nu\bar{\nu}$)

6.2.1 Event selection (Cut-based only)

The event selection cuts are listed below in sequence.

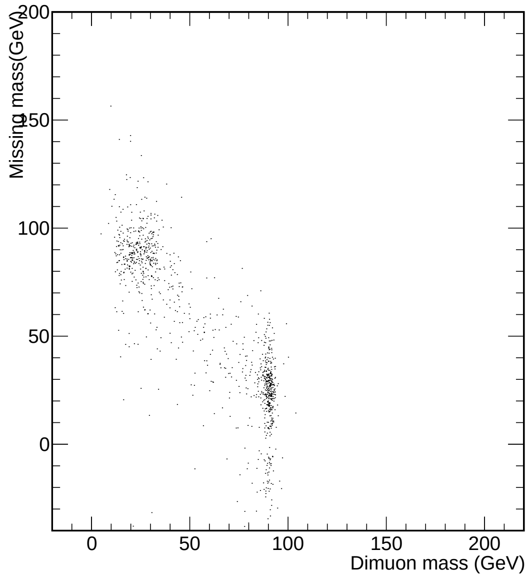

Figure 77: Missing mass vs dimuon invariant mass.

- $M_{miss} < M_{dimuon}$: the dimuon invariantmass is greater than the missing mass.

- $40 < N_{pfo} < 95$: Number of Prticle Flow Objects should be in this range.

Table 28: Cut flow table for $qq\mu\mu\nu\nu$ channel

Cut	Signal	ZH Background	2f Background	4f Background	$\frac{S}{\sqrt{S+B}}$
$Expected$	20254.08±142.32	1140511±1067	801811977±28316	107203890±10353	
$Pre-selection$	826.57±28.75	30494 ±174	480828±693	515424±717	
$Signal\ or\ not$	203.35±14.26	30291 ±174	480828±693	515424±717	
$M_{missing} < M_{dimuon}$	108.36±10.41	27112 ±164	462222±679	474655±688	0.1104
$N(pfo)$	96.21 ±9.81	17726 ±133	10817 ±104	290704±539	0.1702
M_{dijet}	87.7 ±9.36	3248 ±56	14 ±3	225594±474	0.1833
M_{dimuon}	74.94 ±8.66	2356 ±48	7 ±2	157235±396	0.1875
$M_{missing}$	57.52 ±7.58	1434 ±37	0 ±0	9677 ±98	0.5443
$*cos\ \theta$	57.52 ±7.58	1434 ±37	0 ±0	9677 ±98	0.5443
$cos\theta_{visible}$	54.48 ±7.38	1313 ±36	0 ±0	5748 ±75	0.6459
$Angle_{\mu j}$	48.2 ±6.94	952 ±30	0 ±0	1160 ±34	1.037
M^{rec}_{dimuon}	46.18 ±6.8	949 ±30	0 ±0	587 ±24	1.1606
M^{rec}_{dijet}	43.34 ±6.58	733 ±27	0 ±0	472 ±21	1.2264
$M_{visible}$	40.71 ±6.38	647 ±25	0 ±0	418 ±20	1.2237
$*P_{visible}$	40.71 ±6.38	647 ±25	0 ±0	418 ±20	1.2237
$*P_{T_{visible}}$	40.71 ±6.38	647 ±25	0 ±0	418 ±20	1.2237
$*E_{leading\ jet}$	40.71 ±6.38	647 ±25	0 ±0	418 ±20	1.2237
$*P_{T_{leading\ jet}}$	40.71 ±6.38	647 ±25	0 ±0	418 ±20	1.2237
$*E_{sub-leading\ jet}$	40.71 ±6.38	647 ±25	0 ±0	418 ±20	1.2237
$*P_{T_{sub-leading\ jet}}$	40.71 ±6.38	647 ±25	0 ±0	418 ±20	1.2237
$not\ \mu^+\mu^- HZZ$	35.44 ±5.95	206 ±14	0 ±0	305 ±17	1.5143
$not\ \nu\nu HZZ$	35.44 ±5.95	206 ±14	0 ±0	305 ±17	1.5143±0.3527

Table 29: Remained backgrounds (more than 1 event) after all of cuts applied.

name	scale	final
e2e2h_bb	0.21896	120
e2e2h_cc	0.011032	1
e2e2h_ww	0.08176	55
e2e2h_zz	0.010024	8
qqh_e3e3	0.4844	15
qqh_ww	1.6464	1
zz_sl0mu_up	1.09032214858	85
zz_sl0mu_down	1.08025726079	217
zz_sl0tau_up	1.10880522921	1
zz_sl0tau_down	1.10887174477	1
ww_sl0muq	1.10890944134	1

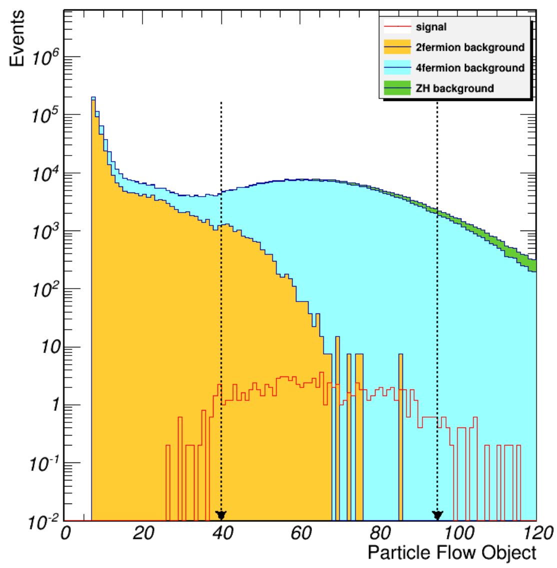

Figure 78: Number of PFOs.

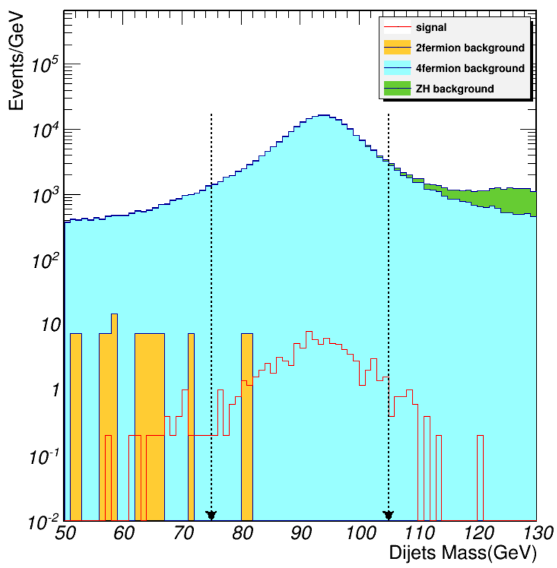

Figure 79: Invariant mass of di-jets.

- $75GeV < M_{dijet} < 105GeV$: the invariant mass of dijet should be in this range.

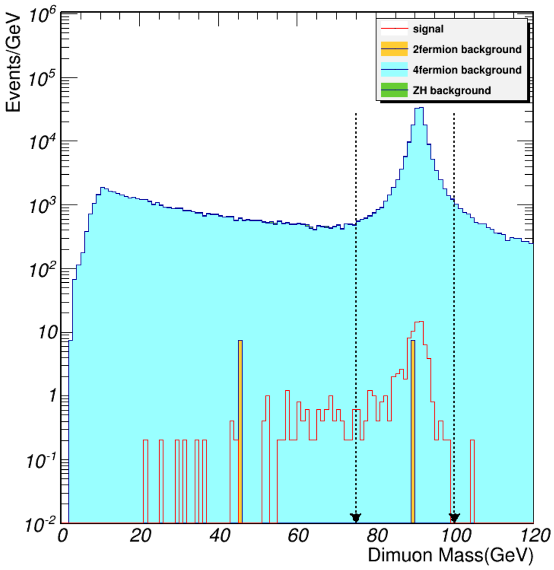

Figure 80: Invariant mass of di-muons.

- $75GeV < M_{\mu^+\mu^-} < 100GeV$: the invariant mass of the dimuon should be in this range.

- $10GeV < M_{visible}^{Recoil} < 50GeV$: the recoil mass of all visible particles should be in this range.

- $-0.95 < cos\ \theta_{visible} < 0.95$: $cos\theta$ of the summation of all visible particles should be in this range.

- $120 < Min\ angle < 170°$: Minimum angle between the two Z(Z*) reconstructed by leptons and jets should be within this range .

- $115GeV < M_{Recoil}^{dimuon} < 155GeV$: the recoil mass of the dimuon should be in this range.

- $110GeV < M_{Recoil}^{dijet} < 140GeV$: the recoil mass of the dijet should be in this range.

- $185GeV < M_{visible} < 215GeV$: the visible mass of all particles should be in this range.

Two additional cuts:

- $M_{dimuon}^{rec} < 122GeV\ or\ M_{dimuon}^{rec} > 128GeV$: To avoid the overlap events with $\mu\mu$HZZ signals.
- $M_{visible} < 122GeV\ or\ M_{visible} > 128GeV$: To remove the overlap events with $\nu\nu$HZZ signals.

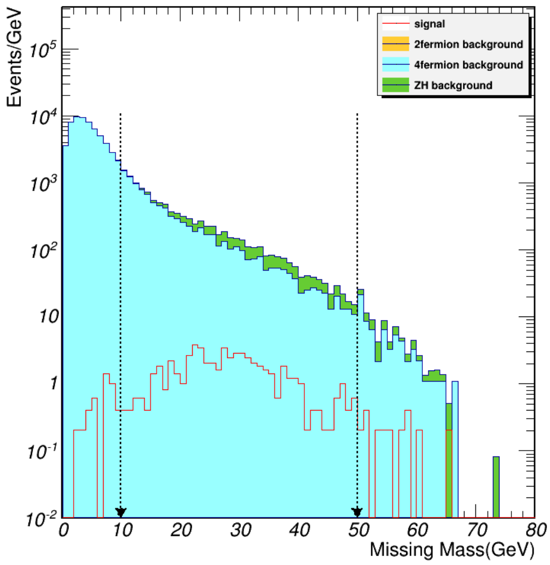

Figure 81: Recoil mass of visible particles.

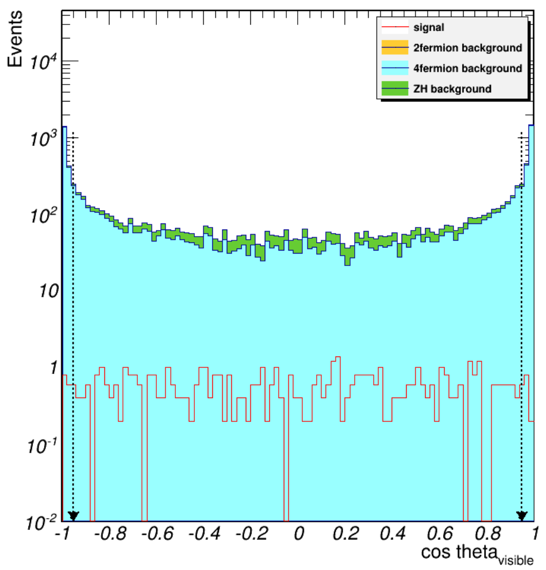

Figure 82: All visible particle $cos\ \theta$

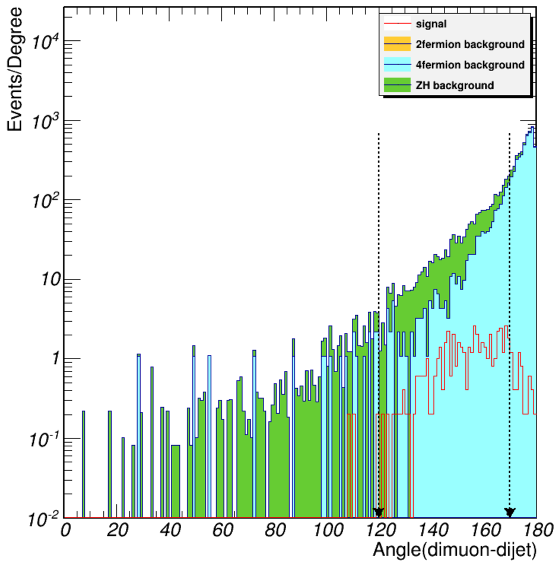

Figure 83: Minimum angle between the two Z(Z*) reconstructed by leptons and jets.

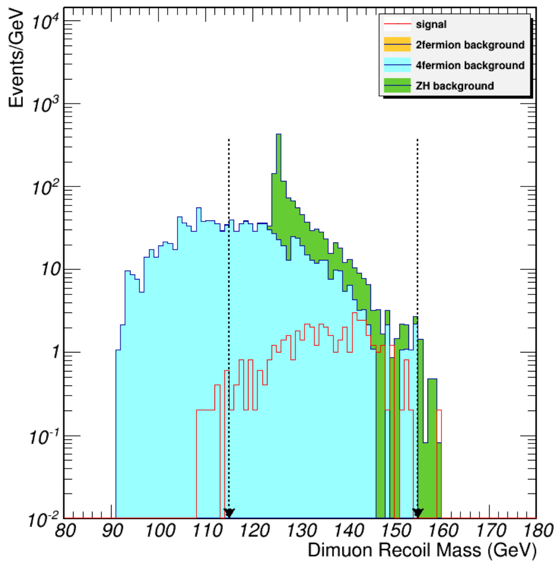

Figure 84: Recoil mass of di-muons.

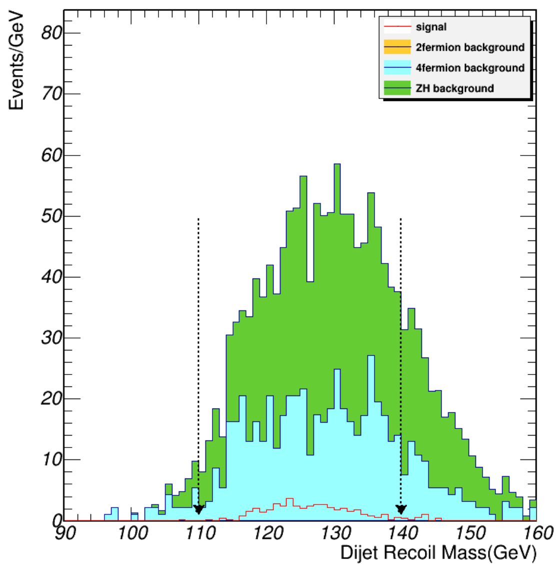

Figure 85: Recoil mass of di-jets.

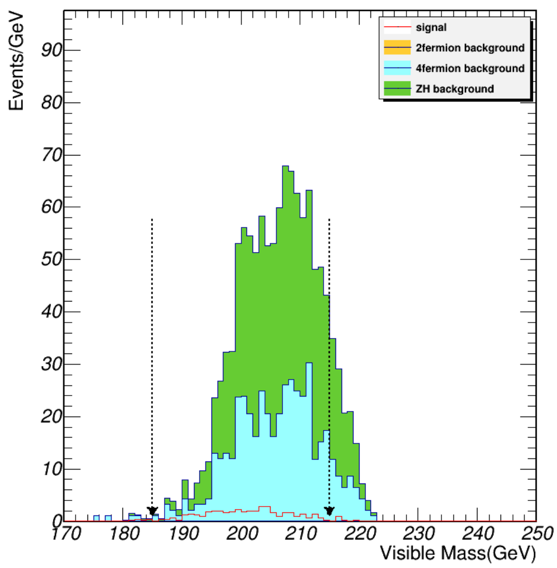

Figure 86: Visible mass of all particles.

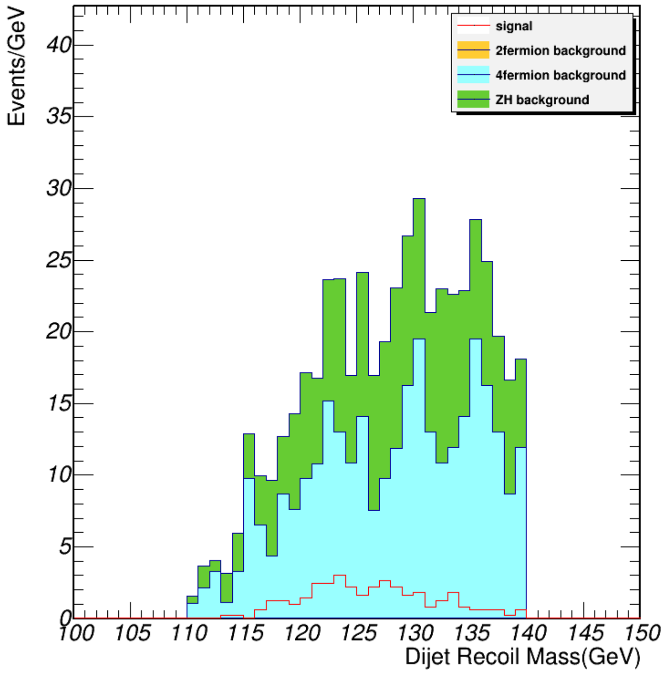

Figure 87: Distribution of the recoil mass of dijet, after all of cuts applied.

6.2.2 Event selection combined with BDT method

- $M_{missing} > M_{dimuon}$: the missing mass is greater than the dimuon invariant mass.
- $35 < N_{pfo} < 100$: Number of PFO is greater than 35 and less than 100.
- $75GeV < M_{dijet} < 110GeV$: the invariant mass of dijet should be in this range.
- $110GeV < M^{rec}_{dijet} < 140GeV$: the recoil mass of the dijet should be in this range.
- $-0.95 < cos\ \theta_{visible} < 0.95$: $cos\theta$ of the summation of all visible particles should be in this range.
- $BDT\ \ score > -0.02$: BDT score greater than -0.02.

The input variable list is: M_{dimuon}, M_{dijet}, $M_{missing}$, N_{pfo}, $cos\ \theta$, $cos\ \theta_{visible}$, $Angle_{\mu^+\mu^- - dijet}$, M^{rec}_{dimuon}, $M_{visible}$, $P_{visible}$, $P_{T_{visible}}$, $E_{leading\ \ jet}$, $P_{T_{leading\ \ jet}}$, $E_{sub-leading\ \ jet}$, $P_{T_{sub-leading\ \ jet}}$. All the variables that are used in cut-based study are in the input variable list for BDT, except M^{rec}_{dijet}, since it is the final observable.

Table 30: Cut flow table for $qq\mu\mu\nu\nu$ channel with BDT

Cut	Signal	ZH Background	2f Background	4f Background	$\frac{S}{\sqrt{S+B}}$
$Expected$	20254	1140511	801811977	107203890	
$Pre-selection$	826	30494	480828	515424	
$Signal\ or\ not$	203	30291	480828	515424	
$M_{missing} < M_{dimuon}$	108	27112	462222	474655	0.1104
$N(pfo)$	103	19806	17185	313602	0.1741
M_{dijet}	97	4531	44	250527	0.1937
M^{rec}_{dijet}	88	3385	7	33021	0.4622
$cos\theta_{visible}$	82	3081	0	18293	0.56
$BDT\ score$	33	161	0	51	2.1536

Table 31: Remained backgrounds (more than 5 event) after all of cuts applied.

name	scale	final
e2e2h_bb	0.21896	24
e2e2h_ww	0.08176	18
qqh_e3e3	0.4844	81
qqh_ww	1.6464	31
zz_sl0mu_down	1.08025726079	27
zz_sl0tau_down	1.10887174477	16

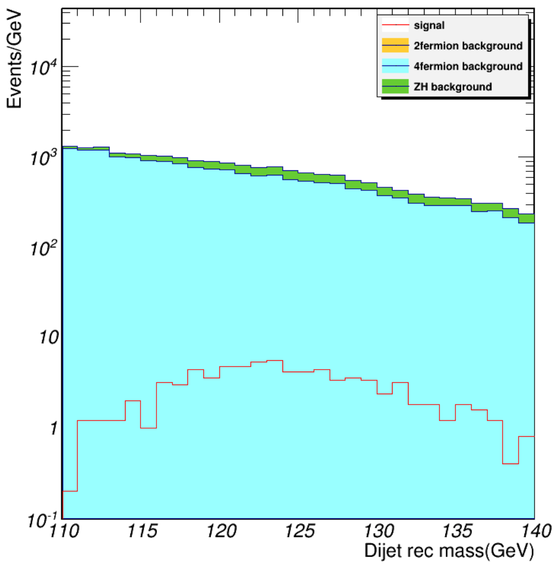

Figure 88: Distribution of the recoil mass of dijet, after the previous cuts applied, before BDT decision applied.

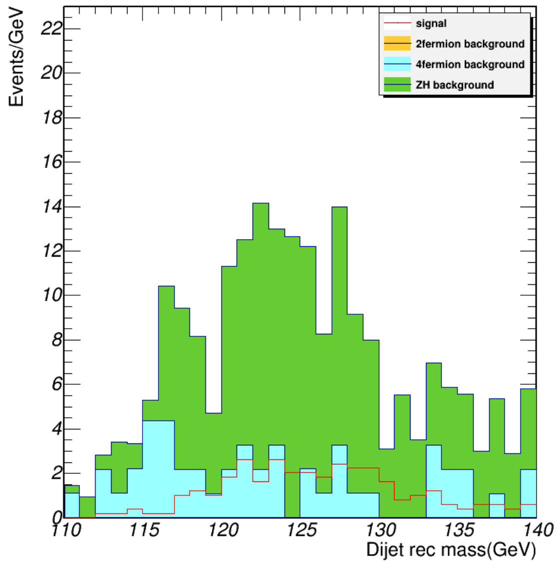

Figure 89: Distribution of the recoil mass of dijet, after all of cuts & BDT decision applied.

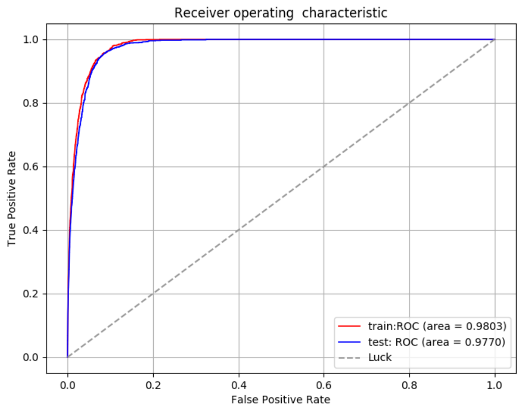

Figure 90: Receiver Operating Characteristic (ROC) curve.

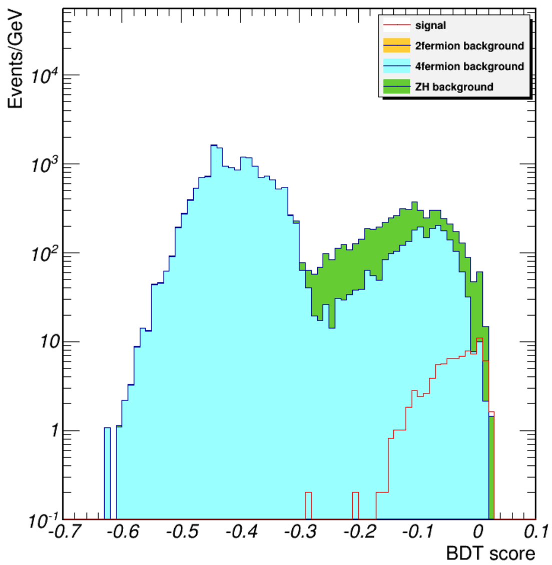

Figure 91: Classifier output distributions of signal and background.

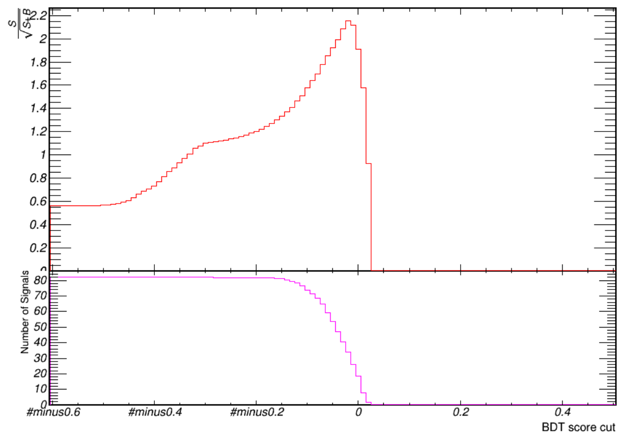

Figure 92: $\frac{S}{\sqrt{S+B}}$ vs BDT score curve.

7 Result

7.1 summary of event selection

7.1.1 summary of event selection (cut-based only)

Table 32: Overview of the requirements applied when selecting events (cut-based).

Pre-selections						
$N(l)$ = 2, where leptons(l) should pass the isolation criteria						
$N(\mu^+) = 1$, $N(\mu^-) = 1$ with $E(\mu^\pm) > 3$ GeV						
$N(jet) = 2$						
Variable	$\mu\mu$H$\nu\nu qq$	$\mu\mu$H$qq\nu\nu$	$\nu\nu$H$\mu\mu qq$	$\nu\nu$H$qq\mu\mu$	qqH$\nu\nu\mu\mu$	qqH$\mu\mu\nu\nu$
$M_{\mu\mu}$ (GeV)	[80,100]	[80,100]	[60, 100]	[10, 60]	[15, 55]	[75, 100]
M_{jj} (GeV)	[15, 60]	[60, 105]	[10, 55]	[60, 100]	[75, 105]	[75,105]
$M_{\mathrm{miss.}}$ (GeV)	[75, 105]	[10, 55]	[75, 110]	[75, 110]	[70, 110]	[10, 50]
$M_{\mu\mu}^{\mathrm{recoil}}$ (GeV)	[110, 140]	[110, 140]	-	-	[175, 215]	[115, 155]
$M_{\mathrm{vis.}}$ (GeV)	-	[175,215]	[110, 140]	[110, 140]	[115, 155]	[185, 215]
$M_{\mathrm{jj}}^{\mathrm{recoil}}$ (GeV)	[185,210]	-	-	-	[110, 140]	[110, 140]
N_{PFO}	[20, 90]	[30, 100]	[20, 60]	[30, 100]	[40, 95]	[40, 95]
$\lvert\cos\theta_{\mathrm{vis.}}\rvert$				< 0.95		
$\Delta\phi_{ZZ}$ (degree)	[60, 170]	[60, 170]	< 135	< 135	-	[120, 170]
$\lvert M_{\mathrm{vis.}} - M_{\mathrm{H}}\rvert$ (GeV)	> 3	> 3	-	-	> 3	> 3
$\left\lvert M_{\mathrm{jj}}^{\mathrm{recoil}} - M_{\mathrm{H}}\right\rvert$ (GeV)	> 3	> 3	> 3	> 3	-	-
$\left\lvert M_{\mu\mu}^{\mathrm{recoil}} - M_{\mathrm{H}}\right\rvert$ (GeV)	-	-	> 3	> 3	> 3	> 3

7.1.2 summary of event selection (BDT)

Table 33: Overview of the requirements applied when selecting events (cut-based).

Pre-selections						
$N(l)$ = 2, where leptons(l) should pass the isolation criteria						
$N(\mu^+) = 1$, $N(\mu^-) = 1$ with $E(\mu^\pm) > 3$ GeV						
$N(jet) = 2$						
Variable	$\mu\mu$H$\nu\nu qq$	$\mu\mu$H$qq\nu\nu$	$\nu\nu$H$\mu\mu qq$	$\nu\nu$H$qq\mu\mu$	qqH$\nu\nu\mu\mu$	qqH$\mu\mu\nu\nu$
$M_{\mu\mu}$ (GeV)	[80,100]	[80,100]	-	-	-	-
M_{jj} (GeV)	-	-	-	-	[75, 105]	[75,110]
$M_{\mathrm{miss.}}$ (GeV)	-	-	[75, 110]	[75, 110]	-	-
$M_{\mu\mu}^{\mathrm{recoil}}$ (GeV)	[110, 140]	[110, 140]	-	-	-	-
$M_{\mathrm{vis.}}$ (GeV)	-	-	[110, 140]	[110, 140]	-	-
$M_{\mathrm{jj}}^{\mathrm{recoil}}$ (GeV)	-	-	-	-	[110, 140]	[110, 140]
$BDT\ score$	> 0.15	> 0.03	> −0.01	> 0.00	> −0.05	> −0.02
N_{PFO}	[20, 90]	[30, 100]	[20, 60]	[30, 100]	[40, 95]	[35, 100]
$\lvert\cos\theta_{\mathrm{vis.}}\rvert$				< 0.95		

7.2 Final Higgs mass distributions and fitting results.

7.2.1 $\mu\mu\nu\nu qq$ channel

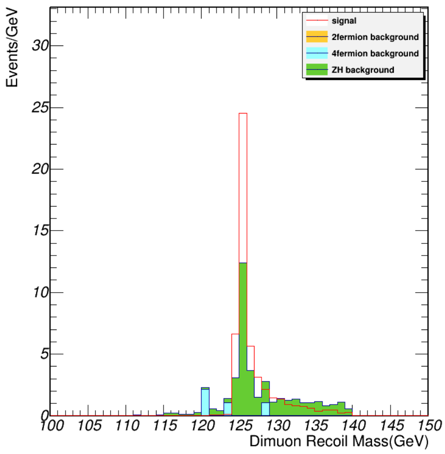

Figure 93: Final Higgs mass distribution of $\mu\mu\nu\nu qq$ (cut-based).

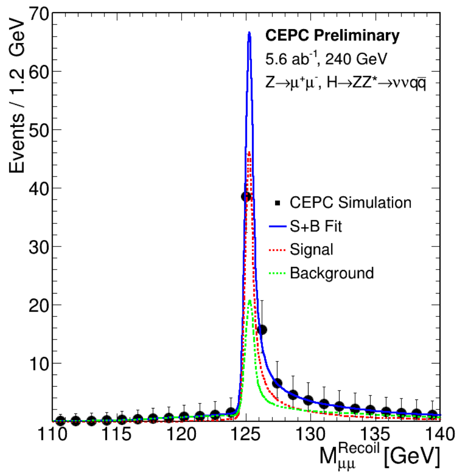

Figure 94: Fit result of $\mu\mu\nu\nu qq$ (cut-based).

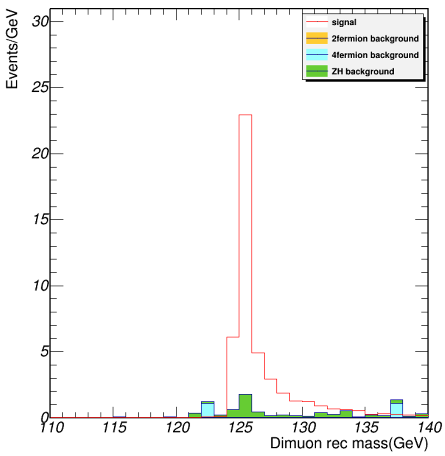

Figure 95: Final Higgs mass distribution of $\mu\mu\nu\nu qq$ (BDT).

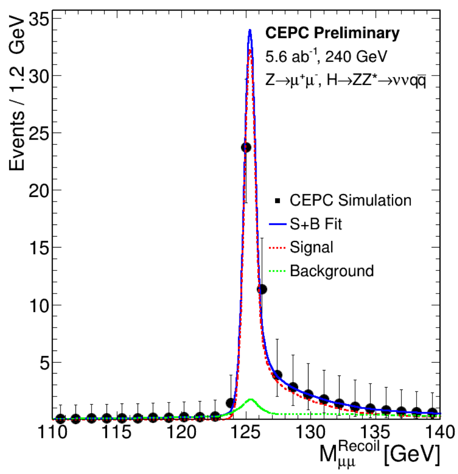

Figure 96: Fit result of $\mu\mu\nu\nu qq$ (BDT).

7.2.2 $\mu\mu qq\nu\nu$ channel

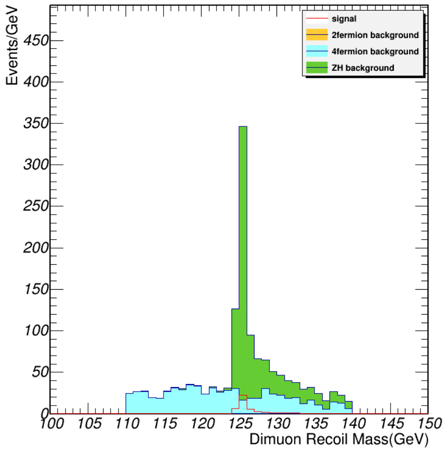

Figure 97: Final Higgs mass distribution of $\mu\mu qq\nu\nu$ (cut-based).

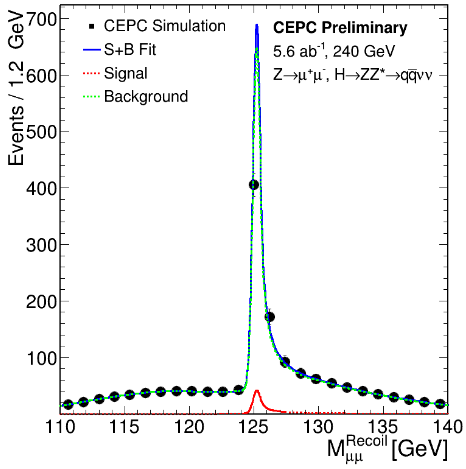

Figure 98: Fit result of $\mu\mu qq\nu\nu$ (cut-based).

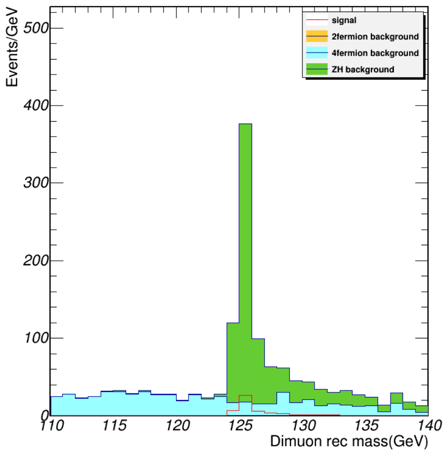

Figure 99: Final Higgs mass distribution of $\mu\mu qq\nu\nu$ (BDT).

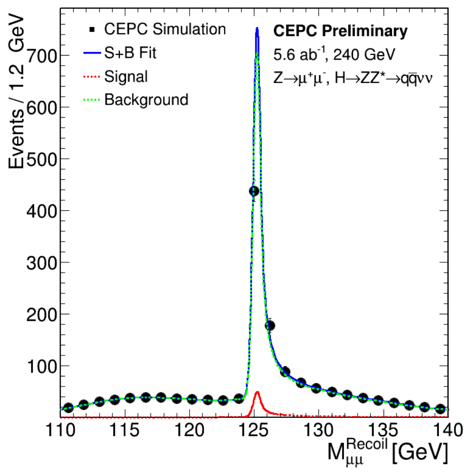

Figure 100: Fit result of $\mu\mu qq\nu\nu$ (BDT).

7.2.3 $\nu\nu\mu\mu qq$ channel

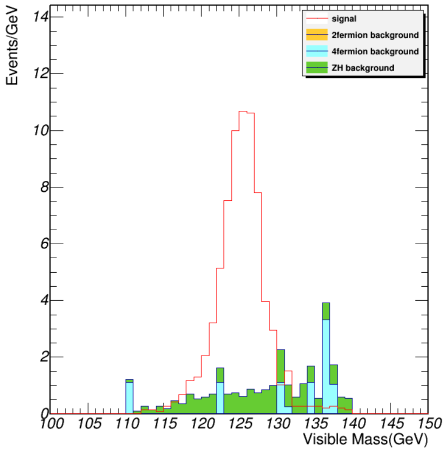

Figure 101: Final Higgs mass distribution of $\nu\nu\mu\mu qq$ (cut-based).

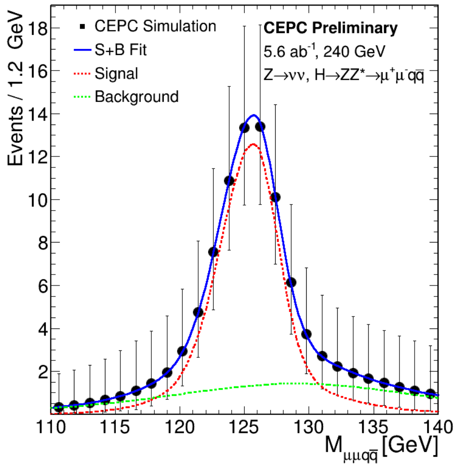

Figure 102: Fit result of $\nu\nu\mu\mu qq$ (cut-based).

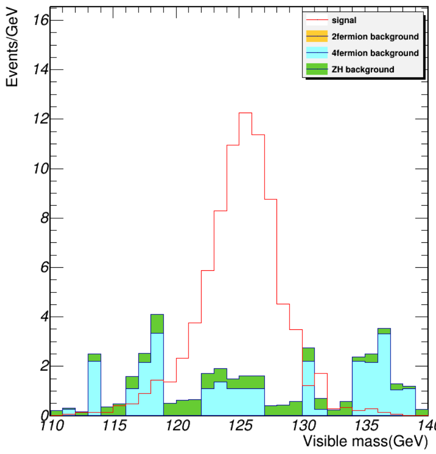

Figure 103: Final Higgs mass distribution of $\nu\nu\mu\mu qq$ (BDT).

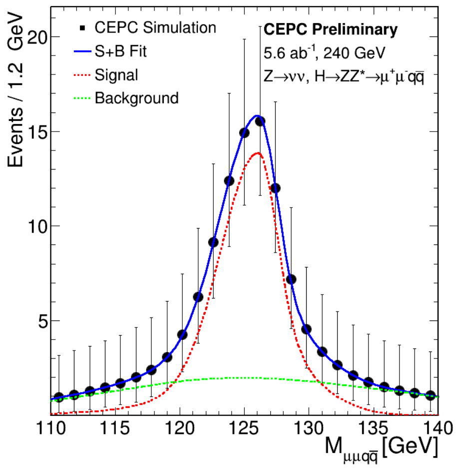

Figure 104: Fit result of $\nu\nu\mu\mu qq$ + $\nu\nu qq\mu\mu$ (BDT).

7.2.4 $\nu\nu qq\mu\mu$ channel

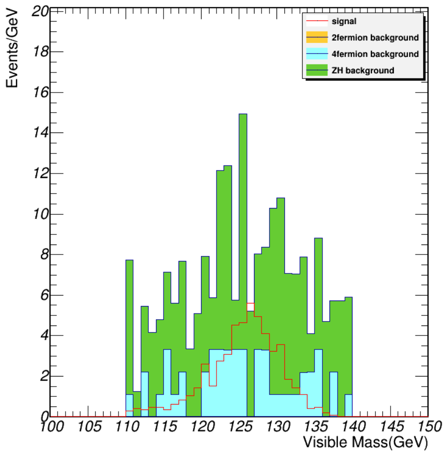

Figure 105: Final Higgs mass distribution of $\nu\nu qq\mu\mu$ (cut-based).

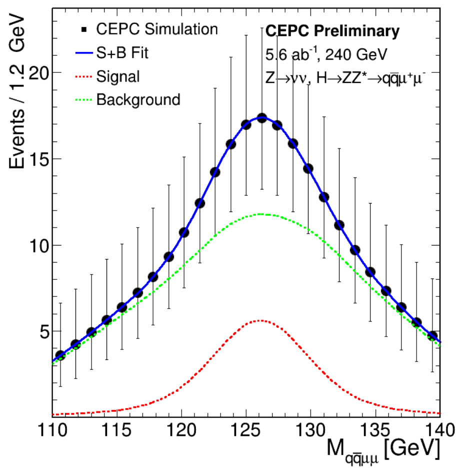

Figure 106: Fit result of $\nu\nu qq\mu\mu$ (cut-based).

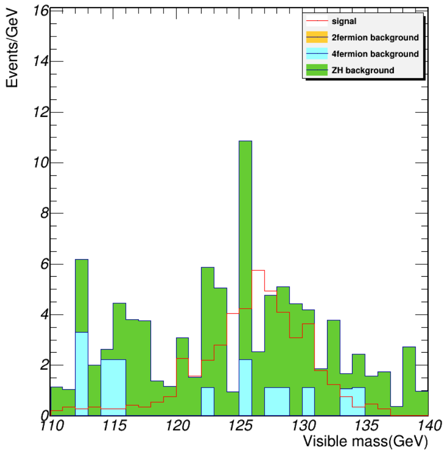

Figure 107: Final Higgs mass distribution of $\nu\nu qq\mu\mu$ (BDT).

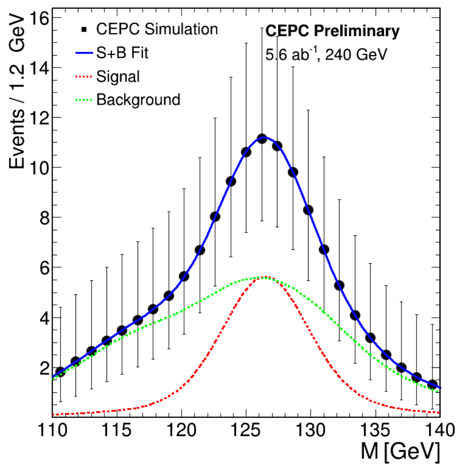

Figure 108: Fit result of $\nu\nu qq\mu\mu$ (BDT).

7.2.5 $qq\nu\nu\mu\mu$ channel

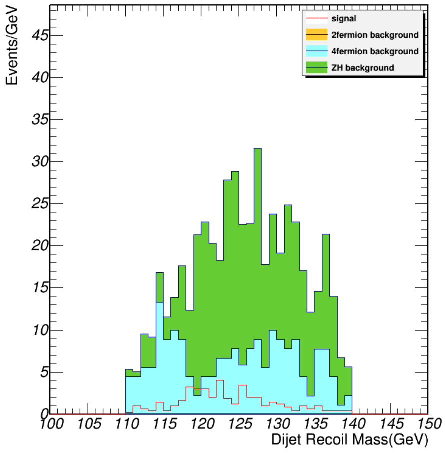

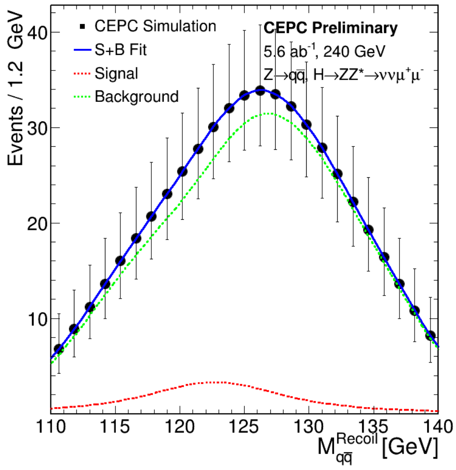

Figure 109: Final Higgs mass distribution of $qq\nu\nu\mu\mu$ (cut-based).

Figure 110: Fit result of $qq\nu\nu\mu\mu$ (cut-based).

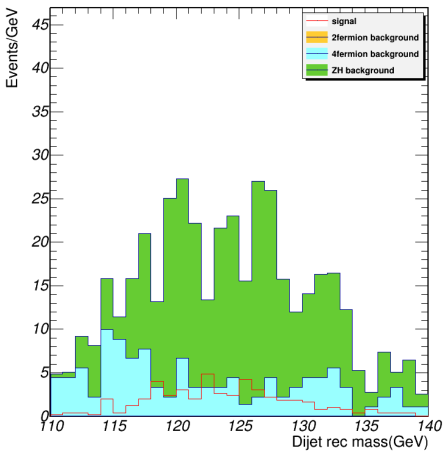

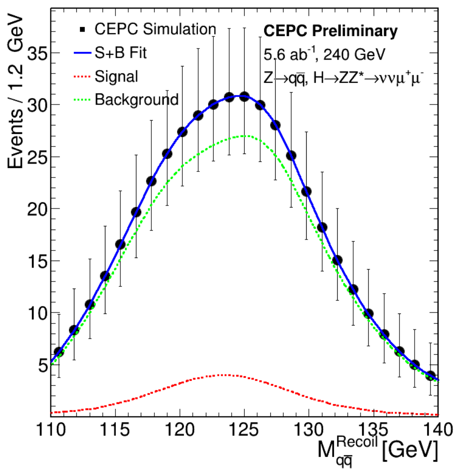

Figure 111: Final Higgs mass distribution of $qq\nu\nu\mu\mu$ (BDT).

Figure 112: Fit result of $qq\nu\nu\mu\mu$ (BDT).

7.2.6 $qq\mu\mu\nu\nu$ channel

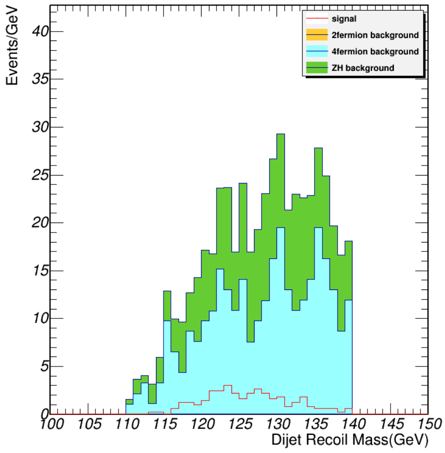

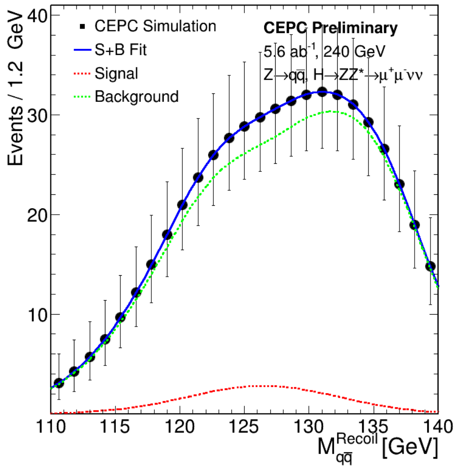

Figure 113: Final Higgs mass distribution of $qq\mu\mu\nu\nu$ (cut-based).

Figure 114: Fit result of $qq\mu\mu\nu\nu$ (cut-based).

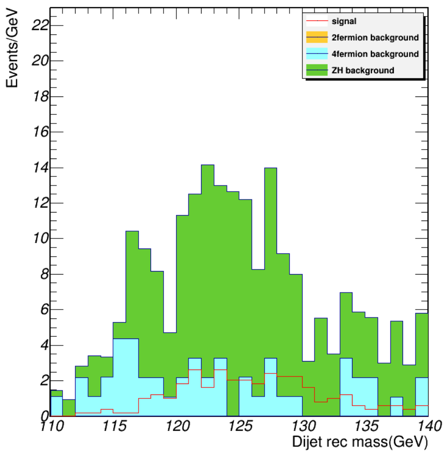

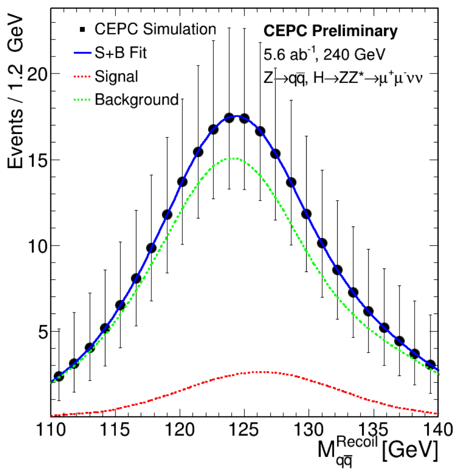

Figure 115: Final Higgs mass distribution of $qq\mu\mu\nu\nu$ (BDT).

Figure 116: Fit result of $qq\mu\mu\nu\nu$ (BDT).

7.3 Calculations

7.3.1 Cut-based calculations

According to the fit results,

$$precision\ of\ \sigma_{ZH} * BR_{signal} : \frac{\Delta\sigma_{ZH} * BR_{signal}}{\sigma_{ZH} * BR_{signal}}$$

is:

$$For\ \mu\mu\nu\nu qq : \ 18.1460\%$$

$$For\ \mu\mu qq\nu\nu : \ 65.3726\%$$

$$For\ \nu\nu\mu\mu qq : \ 13.4518\%$$

$$For\ \nu\nu qq\mu\mu : \ 27.7434\%$$

$$For\ qq\nu\nu\mu\mu : \ 54.2559\%$$

$$For\ qq\mu\mu\nu\nu : \ 63.5335\%$$

Combine results of Precision of Branch ratio of Higgs to ZZ is:

$$9.7121\%$$

Branch ratio of Higgs to ZZ is

$$\frac{N_{signal}}{L\sigma_{ZH} Br_{Z\to\mu\mu} Br_{Z\to\nu\nu} Br_{Z\to jj}\epsilon} :$$

$$For\ \mu\mu\nu\nu qq : \ 2.640\% \pm 0.479\%$$

$$For\ \mu\mu qq\nu\nu : \ 2.639\% \pm 1.725\%$$

$$For\ \nu\nu\mu\mu qq : \ 2.640\% \pm 0.352\%$$

$$For\ \nu\nu qq\mu\mu : \ 2.640\% \pm 0.759\%$$

$$For\ qq\nu\nu\mu\mu : \ 2.640\% \pm 1.432\%$$

$$For\ qq\mu\mu\nu\nu : \ 2.640\% \pm 1.677\%$$

Combine results of Branch ratio of Higgs to ZZ is:

$$2.640\% \pm 0.256\%$$

7.3.2 BDT-based calculations

According to the fit results,

$$precision\ of\ \sigma_{ZH} * BR_{signal} : \frac{\Delta\sigma_{ZH} * BR_{signal}}{\sigma_{ZH} * BR_{signal}}$$

is:

$$For\ \mu\mu\nu\nu qq :\ 15.7951\%$$

$$For\ \mu\mu qq\nu\nu :\ 58.1635\%$$

$$For\ \nu\nu\mu\mu qq :\ 13.0643\%$$

$$For\ \nu\nu qq\mu\mu :\ 23.6133\%$$

$$For\ qq\nu\nu\mu\mu :\ 45.1548\%$$

$$For\ qq\mu\mu\nu\nu :\ 46.0849\%$$

Combine results of Precision of Branch ratio of Higgs to ZZ is:

$$9.4782\%$$

Branch ratio of Higgs to ZZ is

$$\frac{N_{signal}}{L\sigma_{ZH}Br_{Z\to\mu\mu}Br_{Z\to\nu\nu}Br_{Z\to jj}\epsilon} :$$

$$For\ \mu\mu\nu\nu qq :\ 2.640\% \pm 0.417\%$$

$$For\ \mu\mu qq\nu\nu :\ 2.639\% \pm 1.536\%$$

$$For\ \nu\nu\mu\mu qq :\ 2.640\% \pm 0.345\%$$

$$For\ \nu\nu qq\mu\mu :\ 2.640\% \pm 0.623\%$$

$$For\ qq\nu\nu\mu\mu :\ 2.640\% \pm 1.192\%$$

$$For\ qq\mu\mu\nu\nu :\ 2.640\% \pm 1.217\%$$

Combine results of Branch ratio of Higgs to ZZ is:

$$2.640\% \pm 0.250\%$$

Table 34: Cut-based and BDT final precision comparison.

Channel	Cut-based	BDT
$\mu\mu\nu\nu qq$	18.1460%	15.7951%
$\mu\mu qq\nu\nu$	65.3726%	58.1635%
$\nu\nu\mu\mu qq$	13.4518%	13.0643%
$\nu\nu qq\mu\mu$	27.7434%	23.6133%
$qq\nu\nu\mu\mu$	54.2559%	45.1548%
$qq\mu\mu\nu\nu$	63.5335%	46.0849%
Combined	9.7121%	9.4782%

7.3.3 Comparison between cut-based and BDT

Equations used for calculation of precision of Higgs width:

$$\Gamma_H = \frac{\Gamma_{H->ZZ^*}}{Br_{H->ZZ^*}} \propto \frac{\sigma_{ZH}}{Br_{H->ZZ^*}}$$

$$Precision\ of\ \Gamma_H : \frac{\Delta\Gamma_H}{\Gamma_H} = \sqrt{(\frac{\Delta\sigma_{ZH}}{\sigma_{ZH}})^2 + (\frac{\Delta Br_{H->ZZ^*}}{Br_{H->ZZ^*}})^2}$$

8 Backup

8.1 v1.0 result conclusion

summary of event selections for v1.0. Since v1.0 is consistent with v1.1, so we choose the unified version for the baseline cut-based selection.

Table 35: Overview of the requirements applied when selecting events.

Pre-selections						
$N(l)$ = 2, where leptons(l) should pass the isolation criteria						
$N(\mu^+) = 1$, $N(\mu^-) = 1$ with $E(\mu^\pm) > 3$ GeV						
$N(jet) = 2$						
Variable	$\mu\mu$H$\nu\nu qq$	$\nu\nu$H$\mu\mu qq$	$\nu\nu$H$qq\mu\mu$	qqH$\nu\nu\mu\mu$	qqH$\mu\mu\nu\nu$	$\mu\mu$H$qq\nu\nu$
$M_{\mu\mu}$ (GeV)	[80, 100]	[60, 100]	[10, 60]	[15, 55]	[75, 100]	[80, 100]
M_{jj} (GeV)	[15, 60]	[10, 55]	[60, 100]	[75, 105]	[75, 110]	[60, 105]
$M_{\mathrm{miss.}}$ (GeV)	[75, 105]	[75, 110]	[75, 110]	[70, 110]	[10, 50]	[10, 55]
$M_{\mu\mu}^{\mathrm{recoil}}$ (GeV)	[110, 140]	-	[165, 215]	[175, 215]	[115, 155]	[110, 140]
$M_{\mathrm{vis.}}$ (GeV)	-	[110, 140]	[110, 140]	[115, 155]	[185, 215]	[175, 215]
$M_{\mathrm{jj}}^{\mathrm{recoil}}$ (GeV)	[185, 220]	-	-	[110, 140]	[110, 140]	-
N_{PFO}	[20, 90]	[20, 60]	[30, 100]	[40, 95]	[35, 100]	[30, 100]
$\lvert\cos\theta_{\mathrm{vis.}}\rvert$	< 0.95					
$\Delta\phi_{ZZ}$ (degree)	[60, 170]	< 135	< 130	-	[120, 170]	[120, 170]
$\lvert M_{\mathrm{vis.}} - M_{\mathrm{H}}\rvert$ (GeV)	> 3	-	-	> 3	> 3	> 3
$\left\lvert M_{\mathrm{jj}}^{\mathrm{recoil}} - M_{\mathrm{H}}\right\rvert$ (GeV)	> 3	> 3	> 3	-	-	> 3
$\left\lvert M_{\mu\mu}^{\mathrm{recoil}} - M_{\mathrm{H}}\right\rvert$ (GeV)	-	> 3	> 3	> 3	> 3	-

And the precision fitting result for v1.0 is shown below.

$$precision\ of\ \sigma_{ZH} * BR_{signal} : \frac{\Delta\sigma_{ZH} * BR_{signal}}{\sigma_{ZH} * BR_{signal}}$$

is:

$$For\ \mu\mu\nu\nu qq : \ 18.146\%$$

$$For\ \mu\mu qq\nu\nu : \ 65.2495\%$$

$$For\ \nu\nu\mu\mu qq : \ 13.4518\%$$

$$For\ \nu\nu qq\mu\mu : \ 27.8294\%$$

$$For\ qq\nu\nu\mu\mu : \ 54.256\%$$

$$For\ qq\mu\mu\nu\nu : \ 63.9272\%$$

$$Combined : 9.68\%$$

Branch ratio of Higgs to ZZ is:

Table 36: Event selection results for v1.0, mmHqqvv

Cut	Signal	ZH Background	2f Background	4f Background	$\frac{S}{\sqrt{S+B}}$
$Expected$	1000.88±31.64	1140511±1067	801811977±28316	107203890±10353	
$Pre-selection$	616.68±24.83	30494 ±174	480828±693	515448±717	
$Signal\ or\ not$	211.44±14.54	30282 ±174	480828±693	515448±717	
$M_{missing} < M_{dijet}$	103.46±10.17	28674 ±169	365766±604	486638±697	0.1102
$N(pfo)$	100.24±10.01	21686 ±147	12184 ±110	332162±576	0.1657
M_{dimuon}	89.98 ±9.49	16833 ±129	9085 ±95	207927±455	0.186
M_{dijet}	82.95 ±9.11	2768 ±52	52 ±7	173775±416	0.1974
$M_{missing}$	71.56 ±8.46	1679 ±40	14 ±3	13434 ±115	0.5804
$*cos\ \theta$	71.56 ±8.46	1679 ±40	14 ±3	13434 ±115	0.5804
$cos\theta_{visible}$	67.99 ±8.25	1535 ±39	0 ±0	8545 ±92	0.6749
$Angle_{\mu j}$	57.71 ±7.6	1109 ±33	0 ±0	2197 ±46	0.995
M^{rec}_{dimuon}	56.5 ±7.52	1048 ±32	0 ±0	941 ±30	1.2488
$*M^{rec}_{dijet}$	56.5 ±7.52	1048 ±32	0 ±0	941 ±30	1.2488
$M_{visible}$	54.02 ±7.35	930 ±30	0 ±0	790 ±28	1.2823
$*P_{visible}$	54.02 ±7.35	930 ±30	0 ±0	790 ±28	1.2823
$*P_{T_{visible}}$	54.02 ±7.35	930 ±30	0 ±0	790 ±28	1.2823
$*E_{leading\ jet}$	54.02 ±7.35	930 ±30	0 ±0	790 ±28	1.2823
$*P_{T_{leading\ jet}}$	54.02 ±7.35	930 ±30	0 ±0	790 ±28	1.2823
$*E_{sub-leading\ jet}$	54.02 ±7.35	930 ±30	0 ±0	790 ±28	1.2823
$*P_{T_{sub-leading\ jet}}$	54.02 ±7.35	930 ±30	0 ±0	790 ±28	1.2823
$not\ qqHZZ$	46.67 ±6.83	738 ±27	0 ±0	644 ±25	1.2343
$not\ \nu\nu HZZ$	46.67 ±6.83	738 ±27	0 ±0	644 ±25	1.2343±0.3094

Table 37: Event selection results for v1.0, vvHqqmm

Cut	Signal	ZH Background	2f Background	4f Background	$\frac{S}{\sqrt{S+B}}$
$Expected$	6844.99±82.73	1140511±1067	801811977±28316	107203890±10353	
$Pre-selection$	238.62±15.45	30494 ±174	480828±693	515424±717	
$Signal\ or\ not$	226.71±15.06	30268 ±173	480828±693	515424±717	
$M_{dimuon} < M_{dijet}$	101.44±10.07	27436 ±165	58876 ±242	358431±598	0.1521
$N(pfo)$	97.54 ±9.88	20843 ±144	364 ±19	231698±481	0.1939
$M_{missing}$	79.06 ±8.89	769 ±27	37 ±6	2083 ±45	1.4508
M_{dimuon}	78.38 ±8.85	707 ±26	7 ±2	1732 ±41	1.5596
M_{dijet}	68.04 ±8.25	576 ±24	0 ±0	830 ±28	1.7719
$*cos\ \theta$	68.04 ±8.25	576 ±24	0 ±0	830 ±28	1.7719
$cos\theta_{visible}$	64.55 ±8.03	552 ±23	0 ±0	452 ±21	1.9743
$Angle_{\mu j}$	59.83 ±7.73	239 ±15	0 ±0	70 ±8	3.1136
M^{rec}_{dimuon}	58.8 ±7.67	214 ±14	0 ±0	66 ±8	3.1886
$*M^{rec}_{dijet}$	58.8 ±7.67	214 ±14	0 ±0	66 ±8	3.1886
$M_{visible}$	58.11 ±7.62	175 ±13	0 ±0	54 ±7	3.4226
$*P_{visible}$	58.11 ±7.62	175 ±13	0 ±0	54 ±7	3.4226
$*P_{T_{visible}}$	58.11 ±7.62	175 ±13	0 ±0	54 ±7	3.4226
$*E_{leading\ jet}$	58.11 ±7.62	175 ±13	0 ±0	54 ±7	3.4226
$*P_{T_{leading\ jet}}$	58.11 ±7.62	175 ±13	0 ±0	54 ±7	3.4226
$*E_{sub-leading\ jet}$	58.11 ±7.62	175 ±13	0 ±0	54 ±7	3.4226
$*P_{T_{sub-leading\ jet}}$	58.11 ±7.62	175 ±13	0 ±0	54 ±7	3.4226
$not\ \mu^+\mu^-HZZ$	58.11 ±7.62	175 ±13	0 ±0	54 ±7	3.4226
$not\ qqHZZ$	50.72 ±7.12	130 ±11	0 ±0	43 ±6	3.3888±0.4847

Table 38: Event selection results for v1.0, qqHmmvv

Cut	Signal	ZH Background	2f Background	4f Background	$\frac{S}{\sqrt{S+B}}$
$Expected$	20254.08±142.32	1140511±1067	801811977±28316	107203890±10353	
$Pre-selection$	826.57±28.75	30494 ±174	480828±693	515424±717	
$Signal\ or\ not$	203.35±14.26	30291 ±174	480828±693	515424±717	
$M_{missing} < M_{dimuon}$	108.36±10.41	27112 ±164	462222±679	474655±688	0.1104
$N(pfo)$	103.09±10.15	19686 ±140	16961 ±130	313555±559	0.1742
M_{dijet}	97.83 ±9.89	4453 ±66	37 ±6	250524±500	0.1937
M_{dimuon}	83.85 ±9.16	3393 ±58	14 ±3	174150±417	0.1989
$M_{missing}$	64.81 ±8.05	1923 ±43	7 ±2	11132 ±105	0.5657
$*cos\ \theta$	64.81 ±8.05	1923 ±43	7 ±2	11132 ±105	0.5657
$cos\theta_{visible}$	60.76 ±7.8	1761 ±41	0 ±0	6827 ±82	0.6533
$Angle_{\mu j}$	53.27 ±7.3	1181 ±34	0 ±0	1264 ±35	1.0655
M^{rec}_{dimuon}	51.24 ±7.16	1178 ±34	0 ±0	661 ±25	1.1786
M^{rec}_{dijet}	48.41 ±6.96	935 ±30	0 ±0	534 ±23	1.2423
$M_{visible}$	45.37 ±6.74	742 ±27	0 ±0	464 ±21	1.2819
$*P_{visible}$	45.37 ±6.74	742 ±27	0 ±0	464 ±21	1.2819
$*P_{T_{visible}}$	45.37 ±6.74	742 ±27	0 ±0	464 ±21	1.2819
$*E_{leading\ jet}$	45.37 ±6.74	742 ±27	0 ±0	464 ±21	1.2819
$*P_{T_{leading\ jet}}$	45.37 ±6.74	742 ±27	0 ±0	464 ±21	1.2819
$*E_{sub-leading\ jet}$	45.37 ±6.74	742 ±27	0 ±0	464 ±21	1.2819
$*P_{T_{sub-leading\ jet}}$	45.37 ±6.74	742 ±27	0 ±0	464 ±21	1.2819
$not\ \mu^+\mu^-HZZ$	39.5 ±6.28	270 ±16	0 ±0	345 ±18	1.5427
$not\ \nu\nu HZZ$	39.5 ±6.28	270 ±16	0 ±0	345 ±18	1.5427±0.3489

$$For\ \mu\mu\nu\nu qq:\ 2.640\% \pm 0.479\%$$

$$For\ \mu\mu qq\nu\nu:\ 2.638\% \pm 1.721\%$$

$$For\ \nu\nu\mu\mu qq:\ 2.640\% \pm 0.352\%$$

$$For\ \nu\nu qq\mu\mu:\ 2.640\% \pm 0.735\%$$

$$For\ qq\nu\nu\mu\mu:\ 2.640\% \pm 1.432\%$$

$$For\ qq\mu\mu\nu\nu:\ 2.640\% \pm 1.677\%$$

Combine results of Branch ratio of Higgs to ZZ is:

$$2.640\% \pm 0.255\%$$

References

[1] ATLAS Collaboration, Phys. Lett. B, **716**: 1-29 (2012), arXiv:1207.7214[hep-ex]

[2] CMS Collaboration, Phys. Lett. B, **716**: 30-61 (2012), arXiv:1207.7235[hep-ex]

[3] ATLAS Collaboration, Phys. Lett. B, **726**: 88-119 (2013), arXiv:1307.1427[hep-ex]

[4] ATLAS Collaboration, Phys. Lett. B, **726**: 120-144 (2013), arXiv:1307.1432[hep-ex]

[5] CMS Collaboration, JHEP, **1306**: 081 (2013), arXiv:1303.4571[hep-ex]

[6] CMS Collaboration, Nature Phys., **10**: (2014), arXiv:1401.6527[hep-ex]

[7] CMS Collaboration, Phys. Rev. D, **92**: 012004 (2015), arXiv:1411.3441[hep-ex]

[8] ATLAS and CMS Collaborations, JHEP, **08**: 045 (2016), arXiv:1606.02266[hep-ex]

[9] ATLAS and CMS Collaborations, Phys. Rev. Lett., **114**: 191803 (2015), arXiv:1503.07589[hep-ex]

[10] ATLAS Collaboration, Projections for measurements of Higgs boson signal strength and coupling parameters with the ATLAS detector at a HL-LHC, ATL-PHYS-PUB-2014-016 (2014) http://cds.cern.ch/record/1956710

[11] CMS Collaboration, Projected Performance of an Upgraded CMS Detector at the LHC and HL-LHC: Contribution to the Snowmass Process, arXiv:1307.7135[hep-ex]. http://www.slac.stanford.edu/econf/C1307292/docs/submittedArxivFiles/1307.7135.pdf